Agricultural and Forest Meteorology 354 (2024) 110098

Contents lists available at ScienceDirect

Agricultural and Forest Meteorology

journal homepage: www.elsevier.com/locate/agrformet

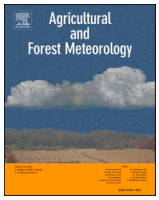

An improved representative of stomatal models for predicting diurnal stomatal conductance at low irradiance and vapor pressure deficit in tropical rainforest trees

Wei Xue [a,b,c], Xue-min He [a,b], Quan Wang [d], Pei-jun Shi [a,b], Guang-hui Lv [a,b], Jian-feng Huang [c], Da Yang [c], Jiao-lin Zhang [c,*]

[a] College of Ecology and Environment, Key Laboratory of Oasis Ecology of Education Ministry, Xinjiang University, Urumqi 830000, PR China
[b] Xinjiang Jinghe Observation and Research Station of Temperate Desert Ecosystem, Ministry of Education, Jinghe 833300, PR China
[c] Xishuangbanna Tropical Botanical Garden, Key Laboratory of Tropical Forest Ecology, Chinese Academy of Sciences, Mengla 666303, PR China
[d] Faculty of Agriculture, Shizuoka University, Shizuoka 422-8529, Japan

ARTICLE INFO

Keywords:
Stomatal conductance
Photosynthesis
Intercellular CO_2 concentration
Vapor pressure deficit
Photosynthetically active radiation
Machine-learning
Random forest
Tropical rainforests

ABSTRACT

The predictions of stomatal conductance (g_{sw}) by the unified stomata optimization (USO) series models in tropical rainforest trees exhibited pronounced biases. However, little attention has been devoted to the structural issues within the USO series models themselves. This study introduced a novel approach by integrating the Farquhar photosynthesis model with the random forest (RF) algorithm to investigate diurnal variations in leaf stomatal responses among six tropical tree species in South China. The results revealed that the USO model and its derivative significantly overestimated g_{sw} when vapor pressure deficit (VPD) and irradiance were low. The overestimation was primarily attributed to the assumption of a linear relationship between g_{sw} and net assimilation rate (A_n) and the issue of unbounded g_{sw} when VPD was low. The relationship between g_{sw} and A_n was indeed non-linear due to a negative correlation between the intercellular: atmospheric CO_2 concentration ratio (C_i/C_a) and irradiance. The relationship between C_i/C_a and irradiance indicated that C_i/C_a was higher at low irradiance, declined and tended to gradually stabilize at high irradiance. An empirical coefficient was determined by using the monthly mean of daytime minimum VPD to represent g_{sw} as finite values at low VPD. The revision achieved a substantial improvement in predictive accuracy of g_{sw} at low VPD while preserving g_{sw} responsiveness under high VPD.

1. Background

Historically, land surface models (LSMs) have primarily employed empirical models of stomatal conductance, such as the Ball–Woodrow–Berry (BWB) model (Ball et al., 1987), and the Ball–Berry–Leuning (BBL) model (Leuning, 1995). However, these models have been increasingly replaced by the unified stomata optimization (USO) model (Medlyn et al., 2011) in LSMs (Bonan et al., 2014; De Kauwe et al., 2015; Rogers et al., 2017; Li et al., 2022). In the BBL model, leaf stomatal conductance to water vapor (g_{sw}) varies linearly with the net assimilation rate (A_n) divided by the CO_2 concentration at the leaf surface (C_s) and the atmospheric vapor pressure deficit (VPD). The significance of the BBL model lies in its expression of the VPD response function, which accounts for the observed hyperbolic variation of g_{sw} in relation to VPD across different species. The USO model was derived mathematically under the assumption of optimal stomatal behavior (Cowan and Farquhar, 1977), wherein stomata control the exchange of water and carbon by aiming to maximize carbon uptake considering a carbon cost to water loss. The USO model shares a similar form with the BBL model, as both models assume a hyperbolic relationship between g_{sw} and VPD and a linear relationship between g_{sw} and A_n under specific environmental conditions. Furthermore, the effects of leaf temperature (T_{leaf}) and photosynthetically active radiation (PAR) on g_{sw} were incorporated into A_n through its dependence on them. However, several studies have shown that these stomatal conductance models had limited predictive capability when it comes to capturing temporal changes in leaf g_{sw} for tropical rainforest trees (Wu et al., 2020; Xue et al., 2022; Davidson et al., 2023). These models tend to have

* Corresponding author.
E-mail address: zjl@xtbg.org.cn (J.-l. Zhang).

https://doi.org/10.1016/j.agrformet.2024.110098
Received 12 October 2023; Received in revised form 15 May 2024; Accepted 30 May 2024
Available online 5 June 2024

significant predictive errors (e.g., root mean square error, RMSE) that are considerably large in comparison to the mean of field observations.

In relation to the unsatisfactory performances of existing stomatal conductance models in tropical rainforest trees, sensitivity evaluations have suggested that model predictability is characterized in regards to the relationships between g_{sw} and environmental factors, which are essential for model parameterization. These factors, primarily concerned soil water potential and leaf traits, exhibit significant variation across multiple organizational scales, including biomes, plant functional types, and species (Egea et al., 2011; Powell et al., 2013; Lin et al., 2015; Miner et al., 2016; Franks et al., 2018; Wu et al., 2020; Vidale et al., 2021; Li et al., 2022). Furthermore, the oversimplification of the model structure poses a challenge as it fails to adequately express the complex response surface of environmental controls on g_{sw} (Ogle and Reynolds, 2002; Lamour et al., 2022; Davidson et al., 2023). Decades of research have shown that stomatal sensitivity to climatic stimuli, such as VPD, can vary among different species (Cunningham, 2004; Oren et al., 1999; Grossiord et al., 2020). Consequently, using a hyperbolic function of VPD to model the stomatal response of distinct species could be an issue (Li et al., 2011). Specifically, Domingues et al. (2014) suggested that the use of a hyperbolic function of VPD may not be appropriate for tropical species that frequently experience low VPD. In fact, when VPD is close to zero, which often occurs in moist rainforests as a result of high relative humidity in air (Graham et al., 2003; Cao et al., 2006; dos Santos et al., 2018), the USO model predicts a conductance value that tends to approach infinity (Medlyn et al., 2011; Li et al., 2022). The USO model significantly overestimated g_{sw} in Panama tropical trees subject to low irradiance, however primarily due to the insensitive responses of g_{sw} to low irradiance (Lamour et al., 2022). The challenge for quantitatively characterizing low VPD impacts on stomatal behavior is that the low VPD condition is usually accompanied by low irradiance. Empirical VPD response functions are based on observed stomatal behavior in response to a normal operating range of the explanatory variable while other variables held constant (Ball et al., 1987; Leuning, 1995; Medlyn et al., 2011), and they serve as a phenomenological representation. The response approach assumes that g_{sw} remains constant at a steady state during measurement settings. However, this approach may not be suitable for examining leaf response under field environmental conditions, as it fails to capture the nonlinear characteristics of diurnal changes in g_{sw}, as frequently encountered (Han et al., 2022; Davidson et al., 2023). It is crucial to address the research gap in understanding the complex relationships between diurnal g_{sw} and explanatory variables. By identifying the limiting factors within these predictor-response relationships, targeted measures can be developed to compensate for potential drawbacks of phenomenological stomatal conductance models.

Non-parametric regression algorithms, such as machine-learning algorithms (MLs) which are statistically ensemble algorithms (Breiman, 1996; 2001; Lary et al., 2016), serve as a convenient interface linking the efficiency of standard statistical techniques with the complexity of physical models (Reichstein et al., 2019). MLs offer an all-purpose non-linear function-fitting capability superior at unraveling complex associations (e.g., non-linear relationships) between a target property and a potentially unlimited number of explanatory predictor variables without requiring explicit knowledge of underlying processes by "letting the data speak for itself" (McCabe et al., 2017; Cao et al., 2020; Zhi et al., 2022). The predictive modelling of MLs is influenced by the type of data and the sample size used for model training (Liu et al., 2021). For instance, the predictive accuracy of the random forest (RF) algorithm for physiological traits in crops is not only related to the number of vegetation indices but also to the size of observed samples throughout crop growing seasons (Jiang et al., 2022). The selection of predictor variables plays a critical role in improving the predictive power of MLs. Recent reviews have identified over 30 alternative models for stomatal conductance (Buckley, 2017; Damour et al., 2010). However, only a small number of these studies have investigated the use of MLs in uncovering the intricate relationships between g_{sw} and explanatory variables (Saunders et al., 2021). Exploring the combination of MLs with the Farquhar-von Caemmerer-Berry photosynthesis model (Farquhar et al., 1980) may inspire ideas for better utilizing field observations to decode and reproduce physiologically based cause-effect relationships.

We recognized that an approach in the community for evaluation of stomatal conductance models is to directly examine the g_{sw} response (Li et al., 2011; Wu et al., 2020; Davidson et al., 2023); namely, stomatal conductance models are not coupled with the Farquhar photosynthesis model (hereinafter, the uncoupled stomatal conductance models). The reason they did not usually couple these models is to reduce the model complexity in the application, e.g. in LSMs. To comprehend the predictor-response relationships in a changing climate, coupling stomatal conductance models with the Farquhar photosynthesis model is crucial (Tuzet et al., 2003; Rogers et al., 2017; Dewar et al., 2018; Li et al., 2022). This is due to the fact that the assimilation rate serves as a critical input in stomatal conductance models (Ball, 1988), and the significance of coupled stomatal conductance models in understanding the physiological mechanisms responsible for diurnal stomatal conductance responses to environmental changes (Tuzet et al., 2003). In this study, we developed a new coupled interface for the Farquhar photosynthesis model and the stomatal conductance model. Instead of using BBL, USO and its derivative, we employed a data-driven RF algorithm trained with extensive diurnal gas exchange and micrometeorological data. This photosynthesis-RF inference tool combines the biochemical photosynthesis model with the strong statistical functions of the RF algorithm, allowing us to explore the complex predictor-response relationships between g_{sw} and predictor variables. Uncertainties in the Farquhar photosynthesis model and temperature response of photosynthetic parameters can influence g_{sw} predictions, complicating the interpretation of diurnal g_{sw} variations (Zhang et al., 2017; Xue et al., 2022). To compare the predictive performance of the coupled stomatal conductance models and the uncoupled models, we conducted experiments on sunlit leaves of six tropical tree species at the Xishuangbanna Tropical Botany Garden of South China (XTBG) during the dry seasons of 2021 and 2023. In this study, we addressed three specific research questions and evaluated one hypothesis as follows:

(1) How well does the VPD formulation used in BBL and USO series stomatal conductance models perform when predicting the diurnal g_{sw}?
(2) To what extent do variations in the VPD-response relationship among those stomatal conductance models affect the predictive accuracy of diurnal g_{sw}?
(3) How does the temperature response of A_n impact the VPD response when the g_{sw} model is combined with the A_n model?
(4) In tropical trees subject to low VPD and irradiance, the unbounded g_{sw} of stomatal conductance models is an unignorable issue, which may cause significant biases in g_{sw} predictions.

2. Materials and methods

2.1. Descriptions of the Farquhar photosynthesis model

For a given set of environmental conditions, including PAR, T_{leaf}, and atmospheric CO_2 concentration (C_a), A_n in the photosynthesis model is determined by either the Rubisco carboxylation capacity (under low CO_2 concentration) or the rate of regeneration of ribulose-1,5-bisphosphate (RuBP) in relation to the electron transport rate dependent on PAR. The limitation of photosynthesis by a deficiency of inorganic phosphate for photophosphorylation is not typically a limiting factor in tropical forests and has been disregarded (Rogers et al. 2021). The photosynthesis model requires the estimation of three key photosynthetic parameters: the maximum carboxylation rate (V_{cmax}), the maximum electron transport rate (J_{max}), and the mesophyll conductance (g_m). These parameters are usually estimated from the response curve of

A_n to intercellular CO_2 concentration (A_n/C_i) and chlorophyll fluorescence data. V_{cmax}, J_{max}, and g_m are influenced by temperature, and various equations describing this relationship can be found in the literature, such as the one provided by Xue et al. (2022) (*see* also note S1).

The left-hand panel of Fig. 1 illustrates the analytical solution of the Farquhar photosynthesis model. To predict the initial A_n value, micrometeorological variables (PAR, C_a, T_{leaf}, and VPD) and an initial guess of CO_2 concentration inside chloroplasts (C_c) are taken into consideration. The first g_{sw} prediction is generated by a stomatal conductance model that incorporates the first A_n prediction and micrometeorological variables. The first C_c is calculated using Fick's law [$C_c = C_s - A_n(1.56/g_{sw} + 1/g_m)$] and is adjusted if the difference from the initial C_c guess exceeds 0.01 ppm. The iterative process is terminated when the difference between the predicted C_c and the previous prediction is less than 0.01 ppm. The predictions of A_n and g_{sw} at the last step of the iterative processes serve as the model outputs. For more information regarding the model descriptions and execution of the code script please refer to Xue et al. (2022).

2.2. Descriptions of leaf stomatal conductance models

In this study, we examined four stomatal conductance models and presented these models in a chronological order. The first two models, namely the BBL (Eq. (1)) and USO (Eq. (2)) models, are extensively employed in most LSMs. The equations are as follows:

$$g_{sw} = g_0 + a_1 \frac{A_n}{(C_s - \Gamma)(1.0 + VPD/D_0)} \quad (1)$$

where a_1 is the slope parameter (unitless), g_0 is the residual g_{sw} when A_n is zero, C_s is the leaf surface CO_2 concentration, Γ is the leaf CO_2 compensation point, and D_0 is the empirical coefficient (kPa) (Leuning, 1995). When using gas exchange systems (Xue et al., 2022; Davidson et al., 2023), C_s is substituted with ambient CO_2 concentration (C_a).

$$g_{sw} = g_0 + 1.6\left(1.0 + \frac{a_1}{\sqrt{VPD}}\right)\frac{A_n}{C_s} \quad (2)$$

where 1.6 accounts for the ratio of diffusivities for water vapor and CO_2 in air, a_1 is proportional to the combination of the marginal water cost of carbon (λ) and the CO_2 compensation point (Γ). The relationship between the a_1 parameter and the marginal water cost of carbon gain was established in the study of Medlyn et al. (2011). In a recent study by Lamour et al. (2022), the USO model was reformulated to include a squared gross photosynthetic rate (referred to as the USO2022 model). Additionally, the integer 1 was removed from the second term on the right-hand side of the equation in this reformulation, as follows:

$$g_{sw} = g_0 + 1.6\frac{a_1}{\sqrt{VPD}}\frac{A_g^2}{C_s} \quad (3)$$

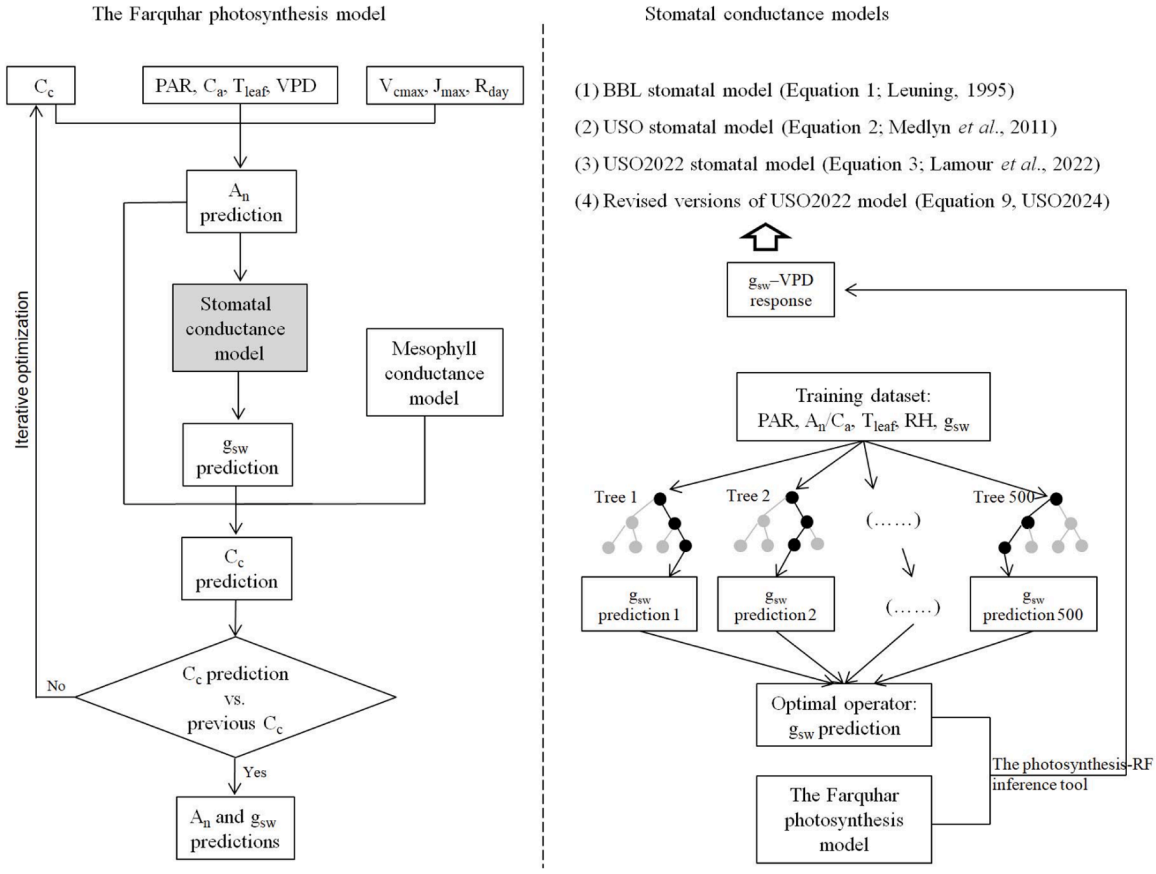

Fig. 1. Analytical roadmaps of the Farquhar photosynthesis model (the left-hand panel) and the leaf photosynthesis-RF inference tool (the right-hand panel). Stomatal conductance models evaluated in this study included the unified stomata optimization model (USO), the Ball–Berry–Leuning model (BBL), the reformed version of the USO model (USO2002) by Lamour et al. (2022), and a reformed version of the USO series models in this study (USO2024). The photosynthesis-RF inference tool is a useful measure to probe complex predictor-response relationships between g_{sw} and predictor variables, which help to develop targeted measures to compensate for potential drawbacks of the phenomenological stomatal conductance models. RF: the random forest algorithm; VPD: leaf-to-air vapor pressure deficit; RH: relative humidity; PAR: photosynthetically active radiation; C_a: ambient CO_2 concentration; T_{leaf}: leaf temperature; R_{day}: dark respiration in the light; A_n: net assimilation rate; g_{sw}: stomatal conductance to water vapor; C_c: CO_2 concentration inside chloroplasts; V_{cmax}: the maximum carboxylation rate; J_{max}: the maximum electron transport rate.

where A_g is the gross photosynthetic rate, expressed by $A_g = A_n + R_{day}$ wherein R_{day} is the leaf dark respiration rate in the light. The USO2022 model was designed to address the non-linear g_{sw}-A_n relationship at low light.

The BBL, USO, and USO2022 models share a common feature, namely the hyperbolic response of g_{sw} to VPD. However, there are significant differences in the expression of VPD in the denominator. The range of the denominator term "1.0+VPD/D_0" in the BBL model is greater than or equal to 1.0, whereas the denominator terms in the USO and USO2022 models are $>$ 0 kPa. As VPD approaches zero, the denominator terms in the USO and USO2022 models become much smaller, resulting in infinite reciprocal values and causing the problem of unbounded g_{sw} estimations at low VPD. The slow changes in g_{sw} observed at low VPD in tropical rainforest trees (Domingues et al., 2014; this study) may be attributable to the inertia of stomatal movement. In order to account for this inertia, VPD is sometimes filtered through a first order delay before it affects stomatal conductance (Lohammar et al., 1980; Leuning, 1995). In most experimental studies, plant g_{sw} response characteristics are typically recorded within a normal operating range of VPD $\geq$ 1.0 kPa, and the hyperbolic response of g_{sw} after the benchmark point of VPD = 1.0 kPa is used to distinguish plant response to increasing VPD among species (Oren et al., 1999; Grossiord et al., 2020). To account for the inertia of stomatal movement at low VPD and the indigenous pattern of g_{sw} response at high VPD $\geq$ 1.0 kPa, the denominator terms of the USO series models (i.e., USO and USO2022) may be revised by adding a delay coefficient (D_0) as follows:

$$\sqrt{VPD + D_0} \geq 1.0 \tag{4}$$

$$D_0 \geq 1.0 - VPD \tag{5}$$

where D_0 is employed to prevent the occurrence of infinitesimal denominator terms, while endeavoring to capture as many variations in VPD across different plant growth habitats. To achieve this, we have defined the VPD of Eq. (5) as the lowest VPD during daytime ($VPD_{min,daytime}$) using the following approach:

$$VPD \approx VPD_{min,daytime} \tag{6}$$

Substitute Eq. (6) into Eq. (5), resulting in a novel formula that establishes the minimum value of D_0 in Eq. (5) as stated below:

$$D_0 = 1.0 - VPD_{min,daytime}, D_0 \geq 0 \tag{7}$$

where the monthly mean value of daytime minimum VPD can be set as the $VPD_{min,daytime}$ threshold. When $VPD_{min,daytime}$ is greater than or equal to 1.0 kPa, the D_0 is zero. According to the convention of the FAO, day length is the time duration of light intensity greater than approximately 30 W m^{-2} (i.e., PAR = 60 μmol m^{-2} s^{-1}). The $VPD_{min,daytime}$ is the minimum VPD observed during the day length.

Based on the inference results, we have proposed revised versions of the USO series models, namely the $USOD_0$ model (Eq. (8)) and the USO2024 model (Eq. (9)). These updated models effectively address the unbounded g_{sw} problem that arises at low VPD, considering variations in local VPD_{min} during daytime for accurate D_0 determination. The revised models are described below:

$$g_{sw} = g_0 + 1.6\left(1.0 + \frac{a_1}{\sqrt{VPD + D_0}}\right)\frac{A_n}{C_s} \tag{8}$$

$$g_{sw} = g_0 + 1.6\frac{a_1}{\sqrt{VPD + D_0}}\frac{A_g^2}{C_s} \tag{9}$$

where Eqs. (8) and (2) are mathematically equivalent, and Eq. (9) is mathematically equivalent to Eq. (3) when D_0 is zero. It should be noted that the D_0 in Eq. (9) is distinct from the one used in the BBL model, which relies on the subjective experience of researchers (Medlyn et al., 2005; Li et al., 2011).

2.3. Descriptions of the leaf photosynthesis-RF inference tool

Solving the unbounded g_{sw} problem using Eqs. (8) and (9) may improve the predictive performance of the USO series models. However, there are still research gaps concerning the response trajectory of g_{sw} to a full range of VPD. In this study, we developed a new photosynthesis-g_{sw} coupled model, replacing the USO series models with a random forest algorithm known as the photosynthesis-RF inference tool (shown in the right-hand panel in Fig. 1). To simplify, we referred to the photosynthesis-RF inference tool as the coupled RF model. The coupled RF model has the advantage of being able to handle large datasets by utilizing a large number of decision trees and nonlinear regression trained on high-dimensional data. Another advantage is that there are no initial assumptions made about the relationships between g_{sw} and VPD, as well as between g_{sw} and PAR, during the training of the coupled RF model. The optimal configuration of the coupled RF model was achieved through the following four steps: (1) preparation of the training dataset, (2) determination of the number of decision trees (ntree) and the number of nodes (mtry) for optimal performance, (3) comparison of the RF predictive performance with other machine learning models, and (4) customization of predictor variables. Each step will be described in detail below.

(1) The preparation of the training dataset: MLs require a training dataset to establish clear associations between a suit of predictor variables and the target variable. In this study, six predictor variables, namely A_n, C_a, VPD, T_{leaf}, relative humidity (RH), and PAR, that directly impact the variation in g_{sw} were equally applied. The dataset was used without dividing it into training and testing datasets because a larger size of the dataset, the higher the predictive performance would be (Liu et al., 2021; Jiang et al., 2022).

(2) The RF algorithm requires the configuration of two parameters: the number of decision trees (ntree) and the number of nodes (mtry). In the "randomForest" package of the R language, the default setting are ntree = 500 and mtry = the number of input variables divided by 3 (Houborg and McCabe, 2018; Hirigoyen et al., 2022).

(3) The RF algorithm, using the six predictor variables, accounted for 94.5 % of the variations observed in diurnal g_{sw}. Furthermore, when compared to two commonly used MLs, namely the deep neural network (DNN) and the partial least squares regression (PLSR), the RF algorithm demonstrated superior predictive accuracy (*see* note S2).

(4) Customization of predictor variables: A higher generalization level is expected with an increasing number of observable conditions being reflected in the training dataset (Jeong et al., 2016; Houborg and McCabe, 2018). Effective training data should encompass the g_{sw} response across a diverse range of environmental conditions, incorporating both present-day and projected climate scenarios, in order to achieve a more representative synthetic response of g_{sw} to predictors. In diurnal gas exchange measurements, the available range of CO_2 concentration is limited to 400–450 ppm, resulting in an absence of training data for CO_2 enrichments exceeding 500 ppm. A_n can be empirically expressed as g_{sw} times the concentration gradient of CO_2 between ambient and intercellular airspaces, in accordance with Fick's law:

$$A_n = \frac{g_{sw}}{1.6}(C_a - C_i) \text{ or, } g_{sw} = \frac{1.6A_n}{C_a(1 - C_i/C_a)} \tag{10}$$

The Eq. (10) presents a clear relationship between changes in C_a and their impact on g_{sw}, expressed as the ratio of A_n to C_a (A_n/C_a). Consistent

with the USO and BBL models that utilize the A_n/C_a ratio as a means to characterize the combined effect of CO_2 on g_{sw}, the A_n and C_a variables in the training dataset were substituted with the A_n/C_a variable.

2.4. Study site and plant material

Field experiments were conducted in the tropical rainforest ecosystems at the Xishuangbanna Tropical Botanical Garden of the Chinese Academy of Sciences (XTBG), situated at the northern edge of the Asian tropical zone (21°41′N, 101°25′E, 580 m a.s.l.). XTBG experiences a typical monsoon climate, with an average annual temperature of 21.8 °C, and annual maximum and minimum temperatures of 33°C and 11°C, respectively (Cao et al., 2006). The region exhibits distinct dry and wet seasons, with approximately 87 % of the annual rainfall occurring from May to October, and the remaining precipitation falling from November to April during the dry season. Heavy radiation fog is common during the morning hours of the dry season, with an average of 116 foggy days per year (Liu et al., 2004). The average monthly RH is 87 %. In the dry seasons, there is a daytime temperature difference of approximately 15–20°C (*see* note S3).

In March 2021, we conducted measurements on the canopy tops of mature leaves from five dominant tree species at XTBG. We utilized a portable gas-exchange and chlorophyll fluorescence system (GFS-3000 and PAM Fluorometer 3050-F, Heinz Walz GmbH, Effeltrich, Germany) to gather data (Table 1). Following that, in January 2023, we conducted measurements on four species, including one additional species not included in the 2021 experiment (Table 1). To ensure accessibility to the upper canopy leaves, all measurements were taken on young trees using a 2-meter tall tripod. Tree species from different families were deliberately chosen to enhance the diversity of leaf material, considering their morphological and photosynthetic traits. Specifically, we focused solely on sunlit mature leaves in the upper canopy, aiming to minimize the influence of leaf phenology and canopy environments on variations in field-measured g_{sw}.

2.5. Measurements of leaf CO_2 response curve and diurnal gas exchange

The photosynthesis-CO_2 response curves (A_n/C_i, where C_i represents the intercellular CO_2 concentration) were collected under high irradiance conditions (PAR = 1600 μmol m^{-2} s^{-1}) and different leaf temperatures. Two to three leaves were placed into a leaf chamber without shading each other and acclimated for 30 minutes at a CO_2 concentration of 400 ppm, high irradiance, and RH of approximately 60 %. The CO_2 concentration inside the leaf chamber was then manipulated to create a declining gradient, ranging from 1600, 1200, 1000, 800, 600, 400, 200, 100, to 50 ppm. Data were recorded once equilibration was reached at each CO_2 concentration. Simultaneously, chlorophyll fluorescence data were recorded alongside the A_n/C_i curve (Xue et al., 2016; 2022). At least three replications of the A_n/C_i curve were obtained for each measuring leaf temperature, which ranged from 15 to 30/40 °C (Table 1). After completing the A_n/C_i curve, dark respiration rates were recorded at CO_2 = 400 ppm and PAR = 0 μmol m^{-2} s^{-1}. Unfortunately, measurements of leaf gas exchange across a range of VPD values could not be made due to alarms occurring during normal operation of the GFS-300 system caused by condensation inside the instrument.

Diurnal gas exchange measurements were conducted on sunlit and fully-expanded leaves that were adjacent to the leaves used for A_n/C_i measurements. Measurements of diurnal gas exchange in the sampled leaves commenced on the day following the completion of A_n/C_i measurements. A user-defined program was used to command the GFS-3000 system to track ambient PAR and air conditions at one or three-minute intervals. Data recording took place from the early morning until the late afternoon. After enclosing the sampled leaves, a thin layer of vaseline was applied to seal the gasket periphery of the leaf chamber and prevent air leakage. The user-defined program executed automatic calibrations every 15 minutes, following the measurement protocols established in our previous studies on crops, temperate trees, and tropical trees (Xue et al., 2022).

2.6. Parameter settings of the Farquhar photosynthesis model

The V_{cmax} and J_{max} values were estimated simultaneously from A_n/C_i curve data using a Bayesian inversion algorithm (Xue et al., 2022). The variable J method, developed by Harley and Tenhunen (1991), which assimilates chlorophyll fluorescence-gas exchange data, along with its derivative that estimates linear electron transport rate (J_p, Equations S8–S11 in note S1) (Xue et al., 2016), was utilized to estimate g_m. The estimated parameters at each leaf temperature were fit by a peaked Arrhenius function (Equation S6 in note S1) to determine the activation energy (ΔH_a) and entropy of inactivation (ΔS) values for the respective variable. The values of V_{cmax}, J_{max}, and g_m at a standard leaf temperature of 25°C as well as their corresponding ΔH_a and ΔS values in the sampled tree species can be found in Table S2.

The diurnal courses of leaf g_{sw} were predicted using two different models: the photosynthesis-g_{sw} coupled model and the uncoupled stomatal conductance models. In the photosynthesis-g_{sw} coupled model, the unknown A_n parameter was estimated based on the V_{cmax}, J_{max}, and g_m values of the tree species being predicted. On the other hand, the uncoupled stomatal conductance models used the measuring A_n accessed from the portable gas exchange system as the A_n parameter.

2.7. Parameter settings of leaf stomatal conductance models

A diurnal gas exchange survey recorded approximately 400 data points per day for each tree species. We gathered diurnal gas exchange data across all sampled tree species in 2021 and 2023 to estimate the slope parameter (a_1) and the residue parameter (g_0) of stomatal conductance models, as detailed in Table S3. This approach to parameter setting scheme was designated as the non-independent parameterization scheme. Incorporating diurnal g_{sw} values of the target species into parameter estimations of stomatal conductance models may lead to an overstated predictability in estimating diurnal g_{sw} values specifically for that species. Consequently, we performed independent estimations of the a_1 and g_0 parameters by compiling diurnal gas exchange data from

Table 1
Monthly frequency of the A_n/C_i curve measurement at the XTBG 2021 and 2023 dry seasons. Entries in cells represent the number of duplicates in measurement of A_n/C_i curve. T_{leaf}: leaf temperature; CTFS: Center for Tropical Forest Science; XTBG: Xishuangbanna Tropical Botany Garden. NA: not available.

Year	Tree species	CTFS code	Foliage	T_{leaf} for A_n/C_i curve (°C)	January	March
XTBG 2021	*Syzygium polypetaloideum*	Syzypo	Evergreen	15–40	NA	6
	Ormosia henryi	Ormohe	Evergreen	15–40	NA	6
	Elaeocarpus hainanensis	Elaeha	Evergreen	15–40	NA	6
	Ficus tinctoria	Ficuti	Evergreen	15–40	NA	6
	Tabebuia heterophylla	Tabehe	Evergreen	15–40	NA	6
2023	*Elaeocarpus hainanensis*	Elaeha	Evergreen	15–30	4	NA
	Senna siamea	Sennsi	Evergreen	15–30	4	NA
	Syzygium polypetaloideum	Syzypo	Evergreen	15–30	4	NA
	Ficus tinctoria	Ficuti	Evergreen	15–30	4	NA

all species, excluding the species being predicted, as detailed in Table S4. The parameter setting approach excluding the target species was designated as the independent parameterization scheme.

2.8. Parameter settings of a two-leaf one-layer canopy photosynthesis model

To assess the representation of the USO series models at the forest canopy level, it is necessary to upscale the leaf stomatal conductance models to predict canopy stomatal conductance (G_{sw}), transpiration rate (Tr_{canopy}), and gross primary productivity (GPP_{canopy}), and compare them with field observations. Considering the similarity between the responses of Tr_{canopy} and GPP_{canopy} to VPD in a one-layer canopy photosynthesis model (PIXCAN) (Xue et al., 2017) and a multi-layer canopy photosynthesis model (Wang and Leuning, 1998), the PIXCAN model was utilized in this study. The PIXCAN model consists of one layer with two types of leaves: sunlit leaves and shaded leaves. The leaf area index (LAI) is divided into sunlit leaf area and shaded leaf area based on an effective radiation transfer model evaluated by Xue et al. (2016). The PIXCAN model is an extension of previous studies by Harley and Tenhunen (1991), Wang and Leuning (1998), Wang et al. (2003), and Owen et al. (2007). For detailed information on the model structure, please

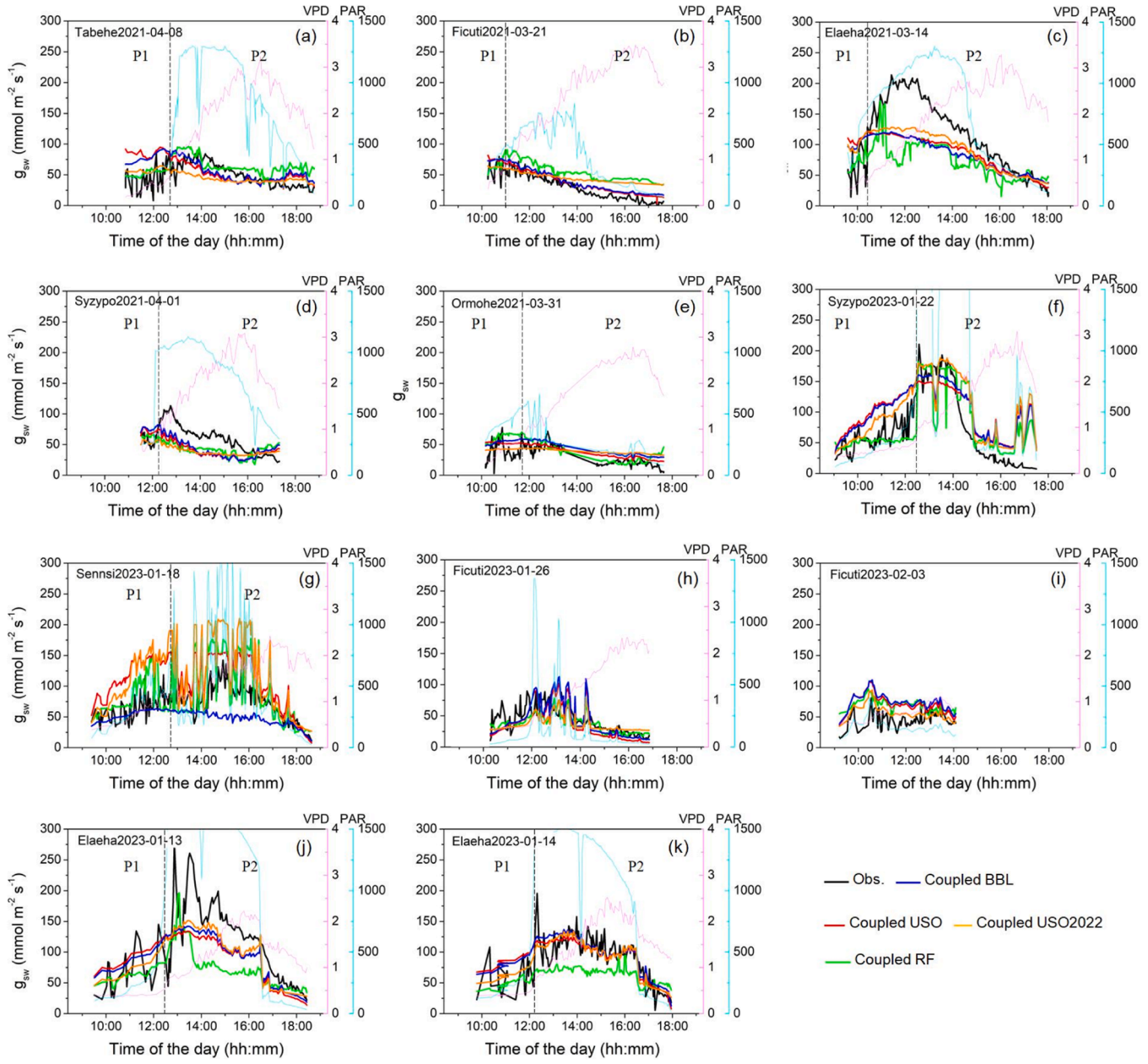

Fig. 2. Comparisons in diurnal leaf stomatal conductance (g_{sw}) of XTBG tropical trees between observations and predictions by the coupled random forest (RF), unified stomata optimization (USO), Ball–Berry–Leuning (BBL), and USO2022 stomatal conductance models (a-k). Parameter settings of stomatal conductance models (the slope parameter a_1 and g_0 values) were obtained using the non-independent parameterization scheme (Table S3). Input variables of the coupled stomatal conductance models were the estimated A_n by the Farquhar photosynthesis model, measuring VPD and atmospheric CO_2 concentration accessed from the portable gas exchange system. The number appending tree species represents the year, month, and day when conducting diurnal gas exchange measurements. The dashed lines demarcated the time periods of the presence of the low VPD when the USO model overestimated g_{sw} (P1). Obs.: observations; A_n: net assimilation rate (μmol m^{-2} s^{-1}); VPD: leaf-to-air water vapor pressure deficit (kPa); PAR: photosynthetically active radiation (μmol m^{-2} s^{-1}). XTBG: the Xishuangbanna Tropical Botany Garden.

refer to those studies. A major improvement in the PIXCAN model is the explicit expression of mesophyll conductance in the Farquhar photosynthesis model (Xue et al., 2017; 2022). Leaf parameters required in the PIXCAN model were obtained from subsections 2.6 and 2.7. Major canopy parameters, such as LAI and leaf inclination angle, were obtained from the study of Jin et al. (2022) and the dataset file deposited in the Asiaflux Database (http://asiaflux.net/), which provides eddy covariance measurements of latent heat flux in the XTBG site in 2003. The calculation procedures for canopy photosynthesis and transpiration as well as PIXCAN model validation are shown in note S4.

2.9. Evaluation of predictive accuracy

The goodness-of-fit of leaf g_{sw} was assessed by comparing the RMSE, R^2, and Nash-Sutcliffe efficiency coefficient (NSE) among BBL, USO, USO2022 and USO2024 models. The NSE values varied from negative infinity to 1. An NSE value closer to 1 indicates that the model is of good quality and high reliability, whereas an NSE value closer to 0 indicates that the simulation result is close to the average level of observations and that the model is credible but with numerous simulation errors. To separate influences of low VPD from irradiance on g_{sw}, we chose the RMSE of the uncoupled USO2022 model as a reference point to measure the errors in g_{sw} estimation resulting from the assumption of a linear relationship between g_{sw} and A_n in the USO model. Similarly, we used the RMSE of the uncoupled USO2024 model as a benchmark to assess the errors in g_{sw} estimation caused by the issue of unbounded g_{sw} in the USO2022 model.

3. Results

3.1. Performance of the coupled stomatal conductance models in predictions of leaf g_{sw}

The diurnal g_{sw} predictions generated by the coupled BBL, USO, USO2022 models, along with the a_1 and g_0 values, and the RF model determined by the non-independent parameterization scheme, are presented in Fig. 2. The diurnal g_{sw} of the Tabehe in April 2021 was captured by the coupled RF model, except for the late afternoon period (Fig. 2a). In addition to the late afternoon period, the coupled USO and BBL models consistently overestimated g_{sw} in the morning under conditions of low VPD (< 0.6 kPa) and low irradiance (< 500 μmol m^{-2} s^{-1}). The section on the left side of the dashed line represents the time period in which g_{sw} was overestimated (referred to as P1), while the rest of the daytime is referred to as P2. The P1 time period accounted for the majority of the morning (Fig. 2a–k). The P1 symbols indicate that the coupled USO and BBL models consistently overestimated g_{sw} in the morning across almost all sampled trees (Fig. 2a–g and i–k). However, an exception was observed in Ficuti on January 26, where no g_{sw} overestimations by the USO and BBL models were detected in the morning when PAR was less than 200 μmol m^{-2} s^{-1}) (Fig. 2h).

The coupled USO2022 model resulted in a significant overestimation of g_{sw} in the morning at three trees: Elaeha, Syzypo, and Sennsi (Fig. 2c, f, and g). The RMSE of the coupled RF model, based on the g_{sw} values for the entire daytime ($RMSE_{P1+P2}$), was 11.5 % lower than the other three coupled models with similar $RMSE_{P1+P2}$ values ($RMSE_{P1+P2}$ = 29.01 mmol m^{-2} s^{-1}) (Table 2). The coupled RF model improved the NSE_{P1+P2} by 14.5 %. The RMSE of g_{sw} values obtained from the P1 block ($RMSE_{P1}$) was 16.92 mmol m^{-2} s^{-1} for the coupled RF model, which was 74.2 % higher than that of the coupled USO2022 model and 123.6 % higher than that of the coupled USO and BBL models. The coupled USO, BBL, and USO2022 models exhibited negative NSE_{P1} values below -1.0, while the coupled RF model had a positive NSE_{P1} value of 0.52. However, the RMSE of g_{sw} values obtained from the P2 block ($RMSE_{P2}$) and the corresponding NSE_{P2} values were similar among all four coupled models.

Fig. S4 displays the diurnal predictions of g_{sw} made by the coupled stomatal conductance models, which were parameterized utilizing the independent parameterization scheme. Consistent with the outcomes of the non-independent parameterization scheme, the coupled BBL, USO, and USO2022 models persistently overestimated g_{sw} under conditions of low VPD and irradiance. The $RMSE_{P1}$ values of the coupled USO, BBL, and USO2022 models displayed a noteworthy difference from the corresponding $RMSE_{P2}$ values, as indicated in Table 2. Across all three models, NSE_{P1} exhibited a departure from zero towards increasingly negative levels.

3.2. Performance of the uncoupled stomatal conductance models in predictions of leaf g_{sw}

Fig. 3 displays predictions of diurnal g_{sw} by the uncoupled stomatal conductance models under the non-independent parameterization scheme. The uncoupled RF model captured changes in diurnal g_{sw} in sampled trees with a high $R^2 = 0.96$ (Table 3). Fig. 3a, d, and e show that the other three uncoupled models adequately captured changes in diurnal g_{sw} in Tabehe, Syzypo, and Ormohe in 2021. Fig. 3b, c, f, g, j, and k indicate that the uncoupled USO model substantially overestimated g_{sw} values in Elaeha in 2021, Syzypo, Sennsi, Ficuti, and Elaeha in 2023, in low VPD and irradiance conditions. In Elaeha, Syzypo, and Sennsi, g_{sw} predictions by the uncoupled USO2022 model fell between the predictions of the uncoupled RF and USO models (Fig. 3c, f, g, j, and k). Figs. 3 and S5 demonstrate that the uncoupled USO and USO2022 models, driven by the independent parameterization scheme, continued to excessively overestimate g_{sw} in the morning under low VPD and irradiance conditions in the same trees. Table 3 confirms that the issue of g_{sw} overestimations in the morning is supported by higher $RMSE_{P1}$ and lower NSE_{P1} values compared to those of the P2 block.

The average $RMSE_{P1+P2}$ for the four uncoupled stomatal

Table 2
Comparisons in predictive accuracy of four coupled stomatal conductance models. D_0 = 2.0 kPa was default setting in the BBL model. Input variables of the coupled stomatal conductance models were the estimated A_n by the Farquhar photosynthesis model, measuring VPD and atmospheric CO_2 concentration accessed from portable gas exchange systems. The right-hand block demarcated by the dashed line in subplots of Fig. 2 was denoted as P1, and the other block denoted as P2. RF: random forest algorithm; USO: the unified stomata optimization stomatal conductance model; BBL: the Ball–Berry–Leuning stomatal conductance model; USO2022: a revised USO model proposed by Lamour et al. (2022); RMSE: root mean square error; NSE: Nash-Sutcliffe efficiency coefficient; R^2: coefficient of determination.

Stomatal conductance models	R^2			RMSE			NSE			Parameterization scheme
	P1+P2	P1	P2	P1+P2	P1	P2	P1+P2	P1	P2	
Coupled BBL	0.64	0.31	0.77	28.87	37.99	25.37	0.63	-1.40	0.75	The non-independent parameterization scheme (Table S3)
Coupled USO	0.61	0.26	0.77	29.62	37.85	26.45	0.61	-1.39	0.73	
Coupled USO2022	0.64	0.27	0.73	28.56	29.48	27.82	0.64	-0.45	0.71	
Coupled RF	0.72	0.54	0.73	25.66	16.92	27.13	0.71	0.52	0.72	
Coupled BBL	0.61	0.19	0.75	30.65	32.51	30.18	0.58	-0.70	0.65	The independent parameterization scheme (Table S4)
Coupled USO	0.54	0.23	0.71	32.05	39.67	29.92	0.54	-1.53	0.66	
Coupled USO2022	0.56	0.18	0.64	31.49	32.30	31.27	0.56	-0.68	0.63	
Coupled RF	0.38	0.07	0.42	37.66	27.67	39.67	0.37	-0.23	0.40	

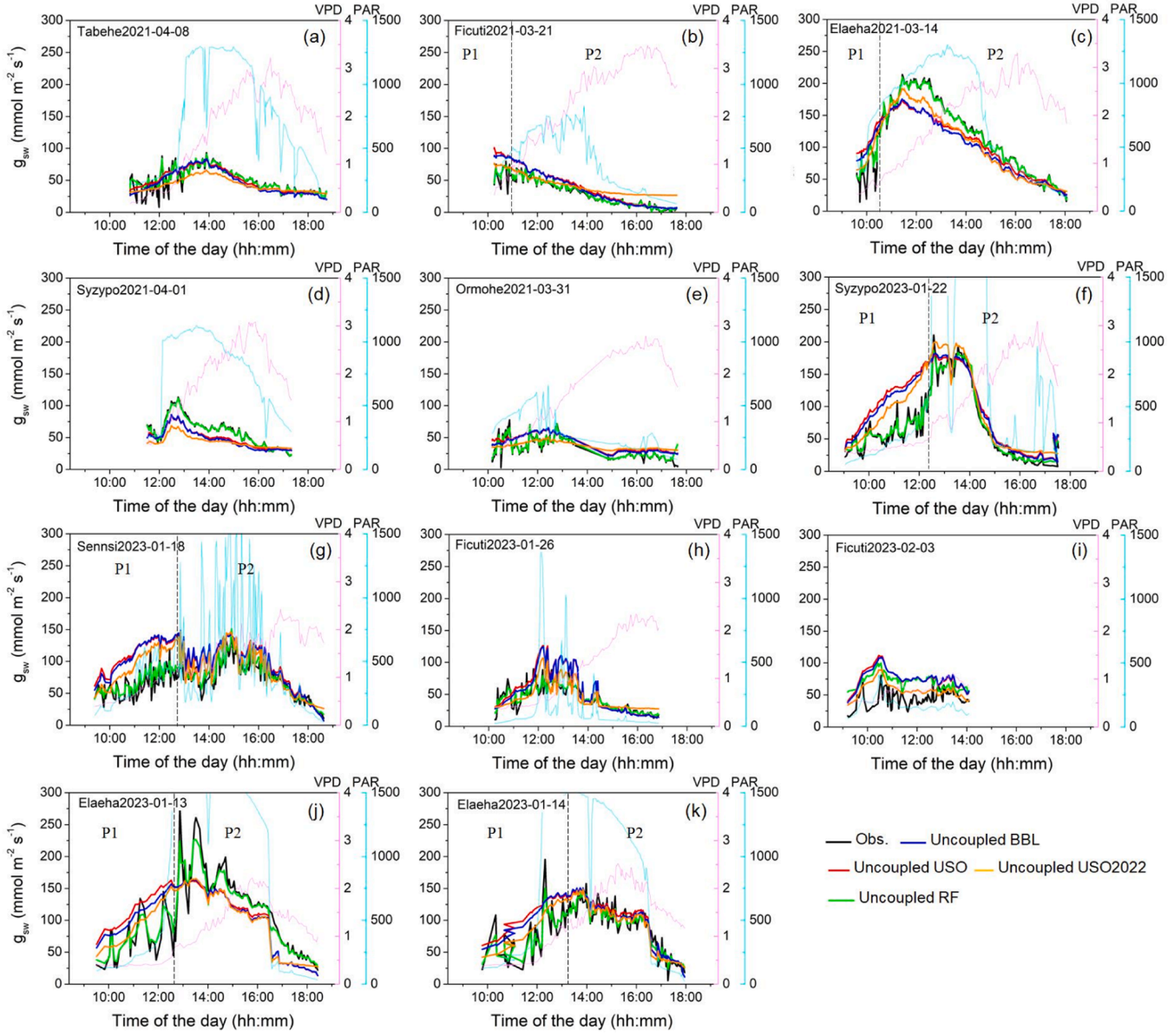

Fig. 3. Comparisons in diurnal leaf stomatal conductance (g_{sw}) of XTBG tropical trees between observations and predictions by the uncoupled random forest (RF), unified stomata optimization (USO), Ball–Berry–Leuning (BBL), and USO2022 stomatal conductance models (a-k). Parameter settings of stomatal conductance models (the slope parameter a_1 and g_0 values) were obtained using the non-independent parameterization scheme (Table S3). Input variables of the uncoupled stomatal conductance models were measuring A_n, VPD, and CO_2 concentration accessed from the portable gas exchange system. The number appending tree species represents the year, month, and day when conducting diurnal gas exchange measurements. The dashed lines demarcated time periods when the USO model overestimated g_{sw}. Obs.: observations; VPD: leaf-to-air water vapor pressure deficit (kPa); PAR: photosynthetically active radiation (μmol m^{-2} s^{-1}). XTBG: the Xishuangbanna Tropical Botany Garden; A_n: net assimilation rate (μmol m^{-2} s^{-1}).

conductance models, which were subjected to the non-independent parameterization scheme, was 18.17 mmol m^{-2} s^{-1} (Table 3). This value was 35.5 % lower compared to the coupled stomatal conductance models. Similarly, the average $RMSE_{P1+P2}$ for the uncoupled models, subject to the independent parameterization scheme, was reduced by 23.6 %. These findings indicate that uncertainties in estimating photosynthesis in the Farquhar model, such as the temperature response of photosynthesis and parameter settings, have a significant impact on the predictive accuracy of stomatal conductance models. However, the overestimation of g_{sw} observed in the USO series models under low VPD and irradiance conditions was not related to these uncertainties.

3.3. Predictor-response relationships between leaf g_{sw} and predictor variables

Predictor-response curves provide crucial insight into the physiological mechanisms underlying the issue of g_{sw} overestimation at low VPD and irradiance levels. The g_{sw}-PAR relationships derived from the coupled BBL and USO models exhibited a rapid increase in g_{sw} with rising PAR from zero, reaching saturation at relatively low PAR values (approximately 300 μmol m^{-2} s^{-1}, Fig. 4a). The predicted g_{sw} values within the PAR range of 100–300 μmol m^{-2} s^{-1} were 11 % and 21 % lower in the coupled USO2022 model compared to the coupled BBL and USO models, respectively (Fig. 4a). The RF-predicted g_{sw} values within the PAR ranges of 100–600 μmol m^{-2} s^{-1} were 19 % and 29 % lower compared to the coupled BBL and USO models, respectively. The g_{sw}

Table 3
Predictive accuracy of the uncoupled BBL, USO, USO2022, and RF stomatal conductance models. Input variables of the uncoupled stomatal conductance models were measuring A_n, VPD, and CO_2 concentration accessed from portable gas exchange systems. The right-hand block demarcated by the dashed line in subplots of Fig. 3 was denoted as P1, and the other block denoted as P2. USO: unified stomata optimization stomatal conductance model; RF: random forest; USO2022: a revised USO model proposed by Lamour et al. (2022); USO2024: a derivative of the USO2022 model (Eq. (9)); XTBG: the Xishuangbanna Tropical Botany Garden; RMSE: root mean square error; NSE: Nash-Sutcliffe efficiency coefficient; R^2: coefficient of determination.

Stomatal conductance models	R^2			RMSE			NSE			Parameterization scheme
	P1+P2	P1	P2	P1+P2	P1	P2	P1+P2	P1	P2	
Uncoupled BBL	0.78	0.30	0.89	22.44	35.43	17.99	0.78	-1.02	0.87	The non-independent parameterization scheme (Table S3)
Uncoupled USO	0.77	0.28	0.90	22.80	38.41	17.07	0.77	-1.37	0.88	
Uncoupled USO2022	0.82	0.30	0.89	20.46	28.86	17.87	0.81	-0.34	0.87	
Uncoupled RF	0.98	0.77	0.99	7.0	12.44	4.87	0.98	0.75	0.99	
Uncoupled BBL	0.76	0.29	0.88	23.12	35.68	18.92	0.76	-1.05	0.86	The independent parameterization scheme (Table S4)
Uncoupled USO	0.72	0.26	0.85	25.43	35.23	22.46	0.71	-1.0	0.81	
Uncoupled USO2022	0.78	0.29	0.84	22.47	32.11	19.49	0.77	-0.66	0.85	
Uncoupled RF	0.69	0.2	0.74	26.82	26.53	26.87	0.68	-0.13	0.73	
Uncoupled USO2024	0.81	0.29	0.87	20.9	27.10	19.16	0.81	-0.18	0.86	

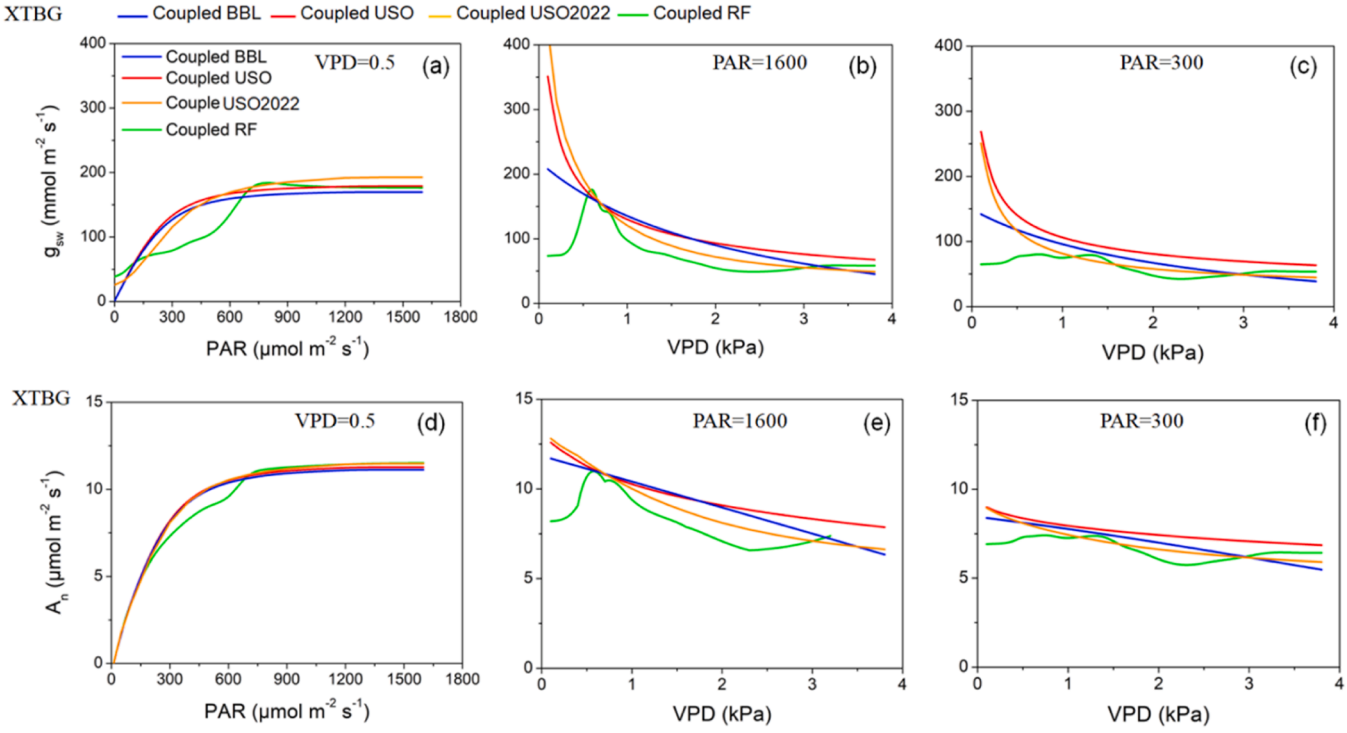

Fig. 4. Synthetic responses of leaf stomatal conductance (g_{sw}, a,b,c) and net assimilation rate (A_n, d,e,f) of XTBG tropical trees to two predictor variables (photosynthetically active radiation-PAR and leaf-to-air vapor pressure deficit-VPD). Synthetic responses of g_{sw} were generated using the coupled stomatal conductance models with the target predictor variable being changed and other predictor variables held constant. Parameters employed to drive the coupled models included PAR = 1600 and 300 μmol m^{-2} s^{-1}, T_{leaf} = 25 °C, CO_2 = 400 ppm, VPD = 0.5 kPa, V_{cmax} = 71.78 μmol m^{-2} s^{-1}, J_{max} = 92.15 μmol m^{-2} s^{-1}, and g_m = 0.08 mol m^{-2} s^{-1}. Temperature response parameters (ΔH_a and ΔS) for V_{cmax}, J_{max}, g_m please referred to Table S2. The slope parameter a_1 and g_0 values referred to Table S3. V_{cmax}: the maximum carboxylation rate; J_{max}: the maximum electron transport rate; g_m: mesophyll conductance; ΔH_a: activation energy; ΔS: entropy of inactivation; XTBG: the Xishuangbanna Tropical Botany Garden.

predictions at low PAR values made by the coupled USO2022 model fell between the predictions of the coupled USO and RF models. The g_{sw} values at PAR = 0 μmol m^{-2} s^{-1} were similar in the coupled RF and USO2022 models (30 mmol m^{-2} s^{-1}), whereas it approached zero in the coupled USO model.

The responses of g_{sw} to VPD were represented by hyperbolic decay models with varying rates within the coupled BBL and USO series models (Fig. 4b). The g_{sw} values predicted by the coupled USO, USO2022, and BBL models at a VPD of 0.5 kPa were 178, 192, and 151 mmol m^{-2} s^{-1}, respectively, and decreased to 120 mmol m^{-2} s^{-1} as the VPD doubled. In contrast to the coupled USO series models, the g_{sw} values predicted by the coupled RF model initially increased and reached a peak of 180 mmol m^{-2} s^{-1} at a VPD of 0.6 kPa, after which it rapidly declined (Fig. 4b). The relationship between g_{sw} and VPD under a PAR of 300 μmol m^{-2} s^{-1} was consistent in the coupled RF model, while it still followed an exponential decay trajectory in the coupled USO series models (Fig. 4c). In Fig. 4c, the g_{sw} values of the USO series models at a VPD of 0.5 kPa were approximately 130 mmol m^{-2} s^{-1}, which were 33 % higher than those of the coupled RF model.

The response trajectory and absolute A_n values of the coupled BBL, USO, and USO2022 models (Fig. 4d) were highly analogous in terms of A_n-PAR relationships, exhibiting relatively higher A_n values at the range of 300–600 μmol m^{-2} s^{-1} by 8 % compared to the coupled RF model. The coupled RF model illustrated an A_n-VPD relationship that demonstrated

an increase in A_n at low VPD levels, reaching a peak around 0.5 kPa, and subsequently decreasing (Fig. 4e). Conversely, the coupled USO series models portrayed an exponential decline in A_n values throughout the entire VPD axis domain. Under low irradiance conditions (PAR = 300 μmol m^{-2} s^{-1}), the coupled RF model displayed A_n values that were 30 % lower than the coupled USO series models at VPD < 0.5 kPa (Fig. 4f).

The g_{sw}-A_n relationships subject to low and high VPD conditions are depicted in Fig. 5. In the results obtained from the coupled BBL, USO, and $USOD_0$ models, g_{sw} showed a remarkable linear increase with A_n under both low and high VPD conditions (Fig. 5a and b). However, the g_{sw}-A_n relationship became non-linear in the coupled RF model, exhibiting minimal changes in g_{sw} at a PAR value of 200 μmol m^{-2} s^{-1} when VPD was set at 0.5 kPa (Fig. 5a), and approximately 120 μmol m^{-2} s^{-1} when VPD was set at 2.0 kPa (Fig. 5b). The non-linear characteristic was evident in the coupled USO2022 and USO2024 models, which displayed similar values to the coupled RF model for PAR values greater than the transition point where nonlinearity appeared. Under both low and high VPD conditions, the residual g_{sw} values of leaves in the dark approached zero in the coupled USO and $USOD_0$ models, whereas it was approximately 20 mmol m^{-2} s^{-1} in the coupled USO2022 and USO2024 models.

The ratio of intercellular and ambient CO_2 concentrations (C_i/C_a) tends to be higher under low irradiance (< 300 μmol m^{-2} s^{-1}), but it remains lower and constant under high irradiance conditions (Fig. 6a). On the other hand, the USO model predicts a constant value for C_i/C_a at different levels of irradiance (Fig. 6b). The RF, USO2022, and USO2024 models exhibit similar nonlinear correlations between C_i/C_a and PAR, which align with the observations made in the field (Fig. 6b).

The results from the independent parameterization scheme showed that the $RMSE_{P1}$ values for the uncoupled USO model and the uncoupled USO2022 model were 35.23 mmol m^{-2} s^{-1} and 32.11 mmol m^{-2} s^{-1}, respectively (Table 3). The USO model overestimated the amplitude of g_{sw} by 9.7 % due to its assumption of a linear g_{sw}-A_n relationship.

3.4. Performance of the USO2024 model in predictions of leaf g_{sw} and canopy G_{sw}

The monthly $VPD_{min,daytime}$ in January and March was estimated to be 0.4 kPa (Figs. 2 and S3c). Consequently, the D_0 value was determined to be 0.6 kPa based on Eq. (7). The USO model has a strong mathematical similarity with the BBL model and a solid theoretical background. In terms of the g_{sw}-A_n relationship (Fig. 5), the $USOD_0$ model did not differ significantly from the USO model. (Fig. 5). Therefore, the following paragraph presents evaluations exclusively for the USO2022 and USO2024 models.

The g_{sw} tended to approach infinity at VPD values below 0.5 kPa in the coupled USO2022 model, while it was bounded in the coupled USO2024 model (Fig. 7a). It is important to note that the g_{sw} values in the coupled USO2024 model were highly similar to those of the coupled USO2022 model for VPD values above 1.0 kPa, with a difference of less than 8 %. As evidenced by the diurnal g_{sw} in Elaeha trees, the USO2024 model outperformed the USO2022 model in predicting diurnal g_{sw} at low VPD values below 0.5 kPa (Fig. 7b). In the results of the independent parameterization scheme (Table 3), the $RMSE_{P1}$ of the uncoupled USO2024 model was found to be 27.10 mmol m^{-2} s^{-1}. Additionally, the NSE_{P1} of the uncoupled USO2024 model showed improvement to a higher level of 0.81, surpassing the benchmark value of 0.77 in the uncoupled USO2022model. The $RMSE_{P2}$ of the uncoupled USO2024 model was highly similar to that of the uncoupled USO2022 model. It is evident that the USO2022 model overestimated g_{sw} in the morning by 18.5 % due to the issue of unbounded g_{sw}.

Results comparing Tr_{canopy} observations and predictions indicated similar predictive accuracy among the coupled BBL, USO, USO2022, and USO2024 stomatal conductance models (*see* note S4). At the canopy level, the G_{sw}-PAR response curves of the coupled BBL and USO models exhibited steeper increments at low irradiance compared to the coupled USO2022 and USO2024 models (Fig. 8a). The residual G_{sw} was minimal and close to zero in the coupled BBL and USO models, while it was higher in the revised USO models. In contrast to the leaf g_{sw}-VPD response curves, canopy G_{sw} increased with VPD and declined after reaching a peak at VPD levels of 1.0-1.5 kPa in all four stomatal conductance models (Fig. 8b). For high VPD, the USO2024-predicted G_{sw} was positioned between the predictions of the USO and USO2022 models. A linear relationship between Tr_{canopy} and VPD was observed in all four models, with similar Tr_{canopy} values predicted at low VPD (Fig. 8c). At higher VPD levels, the USO2024-predicted Tr_{canopy} ranged between the results of the USO2022 and USO models. The GPP_{canopy}-PAR curves were fully overlapped among the four models (Fig. 8d). As VPD intensity increased, GPP_{canopy} decreased almost linearly (Fig. 8e), with stronger sensitivity observed in the USO2022 models (Fig. 8f). GPP_{canopy} was not sensitive to low VPD levels in the BBL and USO2024 models, but started to decline when VPD exceeded 1.0 kPa (Fig. 8f).

4. Discussions

In this research, the overall prediction accuracy (RMSE) of the USO2024, USO2022, and USO models was 20.9 mmol m^{-2} s^{-1}, 22.47

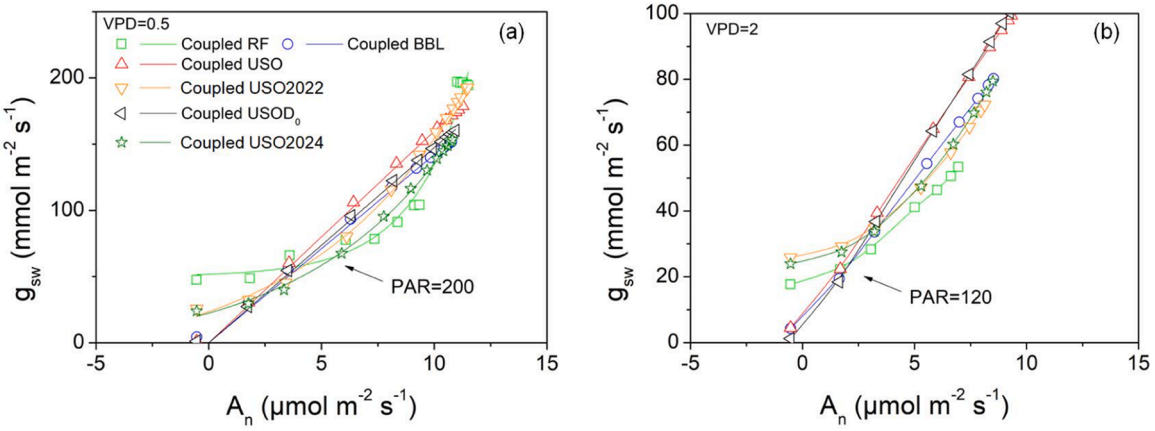

Fig. 5. Relationships between leaf stomatal conductance (g_{sw}) and net assimilation rate (A_n) in trees subject to low and high VPD values (0.5 and 2.0 kPa, a and b). The arrows indicated values of PAR at which the nonlinearity of the g_{sw}-A_n relationship was present. Parameters employed to drive the coupled models included a gradient level of PAR from 0 to 1600 μmol m^{-2} s^{-1}, T_{leaf} = 25 °C, CO_2 = 400 ppm, V_{cmax} = 71.78 μmol m^{-2} s^{-1}, J_{max} = 92.15 μmol m^{-2} s^{-1}, g_m = 0.08 mol m^{-2} s^{-1}. Temperature response parameters (ΔH_a and ΔS) for V_{cmax}, J_{max}, g_m please referred to Table S2. The slope parameter a_1 and g_0 values referred to Table S3. PAR: photosynthetically active radiation; RF: random forest; BBL: Ball–Berry–Leuning model; USO: unified stomata optimization stomatal conductance model; USO2022: a revised USO model proposed by Lamour et al. (2022); $USOD_0$ and USO2024: revised versions of the USO series model (Eqs. (8) and (9)).

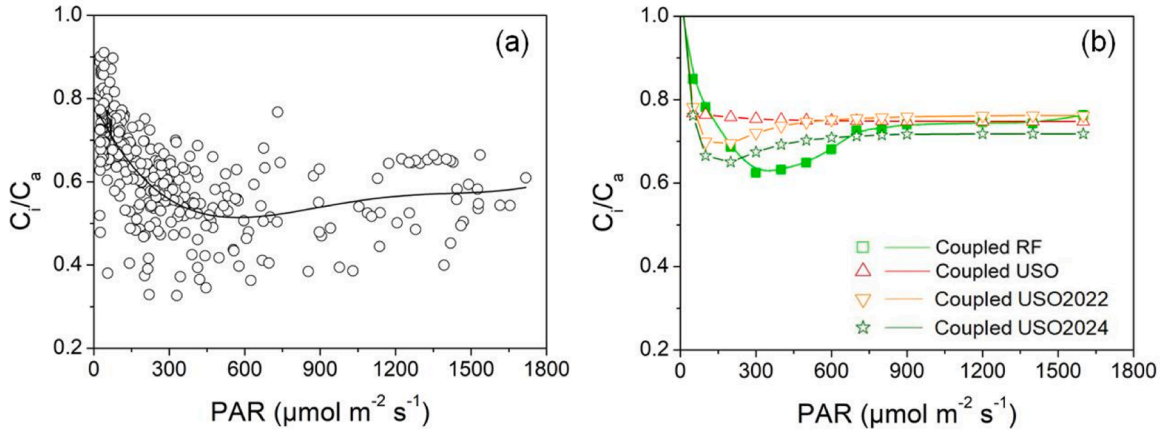

Fig. 6. Relationships between the ratio of leaf intercellular CO_2 concentration to ambient CO_2 concentration (C_i/C_a) and photosynthetically active radiation (PAR). Data applied in subplot (a) were obtained from diurnal measurements of the portable photosynthesis device with the mean value of VPD = 1.3 kPa. C_i/C_a values shown in subplot b were predictions by the coupled stomatal conductance models using Eq. (10). Parameters employed to drive the coupled stomatal conductance models included VPD = 0.5 kPa, T_{leaf} = 25 °C, CO_2 = 400 ppm, V_{cmax} = 71.78 μmol m^{-2} s^{-1}, J_{max} = 92.15 μmol m^{-2} s^{-1}, g_m = 0.08 mol m^{-2} s^{-1}. Temperature response parameters (ΔH_a and ΔS) for V_{cmax}, J_{max}, g_m please referred to Table S2. The slope parameter a_1 and g_0 values referred to Table S3. RF: random forest; USO2022: a revised USO model proposed by Lamour et al. (2022); USO2024: a revised version of the USO2022 model (Eq. (9)).

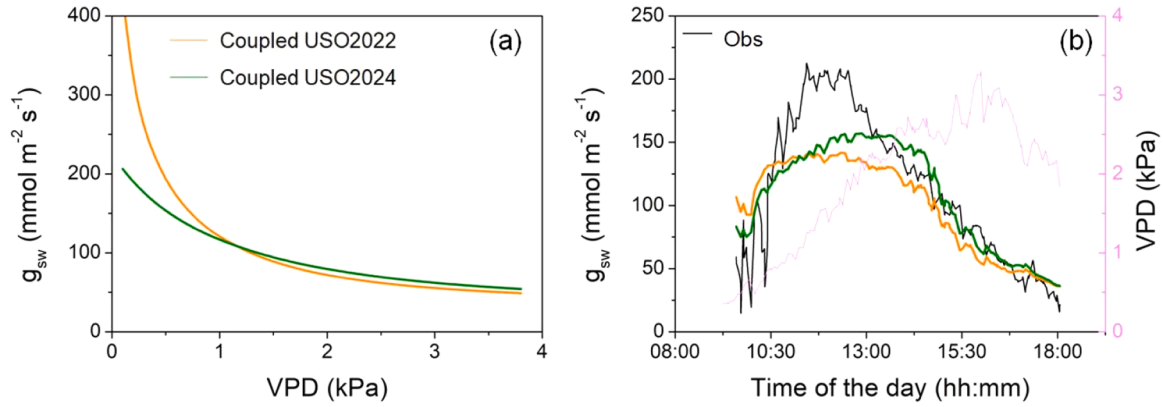

Fig. 7. Comparisons in the g_{sw}-VPD relationship between the coupled USO2022 and USO2024 models (a), and g_{sw} predictions by the two models in Elaeha leaves in 2021 (b). $USOD_0$ and USO2024: revised versions of the USO2022 model (Equations 8 and 9); g_{sw}: stomatal conductance; VPD: vapor pressure deficit; Obs.: observations.

mmol m^{-2} s^{-1}, and 25.43 mmol m^{-2} s^{-1}, respectively (Table 3). The USO series models were ranked based on their RMSE values for diurnal g_{sw}, with the order being USO2024 > USO2022 > USO. The USO2022 model performed better than the USO model due to its consideration of the non-linear relationship between g_{sw} and A_n at low values of PAR. The performance of the USO2024 model was further improved by expressing the bounded g_{sw} at low VPD. The physiological mechanisms underlying the performance of these models will be discussed in the following paragraphs.

The USO model significantly overestimated g_{sw} predictions at low levels of VPD and PAR throughout the morning (Fig. 2). Uncertainties stemming from temperature dependencies of photosynthetic parameters (V_{cmax}, J_{max}, etc.) and g_m can introduce errors in diurnal g_{sw} predictions (Zhang et al., 2017; Xue et al., 2022). Significantly, our findings indicated that the issue of g_{sw} overestimation did not stem from uncertainties in parameter estimations of the Farquhar photosynthesis model. Instead, it suggested that inherent flaws in the USO model led to exaggerated g_{sw} values under low VPD and PAR conditions. Given the regressor and response factor in the USO model, it is necessary to examine the relationships between g_{sw}-A_n and elucidate the response characteristics of these two variables to PAR and VPD. Our observations revealed a non-linear relationship between g_{sw} and A_n at low irradiance, with g_{sw} showing insensitivity to increases in A_n. The specific irradiance at which this nonlinearity emerged partly depended on VPD. Prior studies have documented a non-linear relationship between g_{sw} and A_n under low irradiance conditions (Ball, 1988; Barnard and Bauerle, 2013). A_n exhibited a linear increase with rising PAR, starting from zero and reaching saturation at a relatively low PAR of 300 μmol m^{-2} s^{-1}. The assumption of a linear correlation between g_{sw} and A_n in the USO model led to g_{sw} increasing linearly with both A_n and PAR. Consequently, this resulted in substantial overestimations of diurnal g_{sw} at low PAR values. According to Lamour et al. (2022), the nonlinearity may be attributed to either the suboptimal response of leaves with positive conductance in the absence of light or the shift in biochemical limitation on photosynthesis from RuBP regeneration to Rubisco carboxylation. The structural elements of Eq. (10) suggest that the nonlinear relationship between g_{sw}-A_n could be a result of significant fluctuations in C_i/C_a. Our findings confirmed that the inverse relationship between C_i/C_a and irradiance contributed to the non-linear nature of the g_{sw}-A_n relationship. Plants subjected to low photon flux densities exhibited elevated C_i/C_a levels (Ehleringer et al., 1986; Lamour et al., 2023), while C_i/C_a remained consistently lower at high irradiance, aligning with previous studies on unstressed plants (Wong et al., 1978; Farquhar and Wong, 1984; Dewar et al., 2018) that above an irradiance of around 250 μmol m^{-2} s^{-1}, C_i/C_a tended to be unaffected by changes in irradiance.

There were similarities in the response patterns of C_i/C_a to PAR

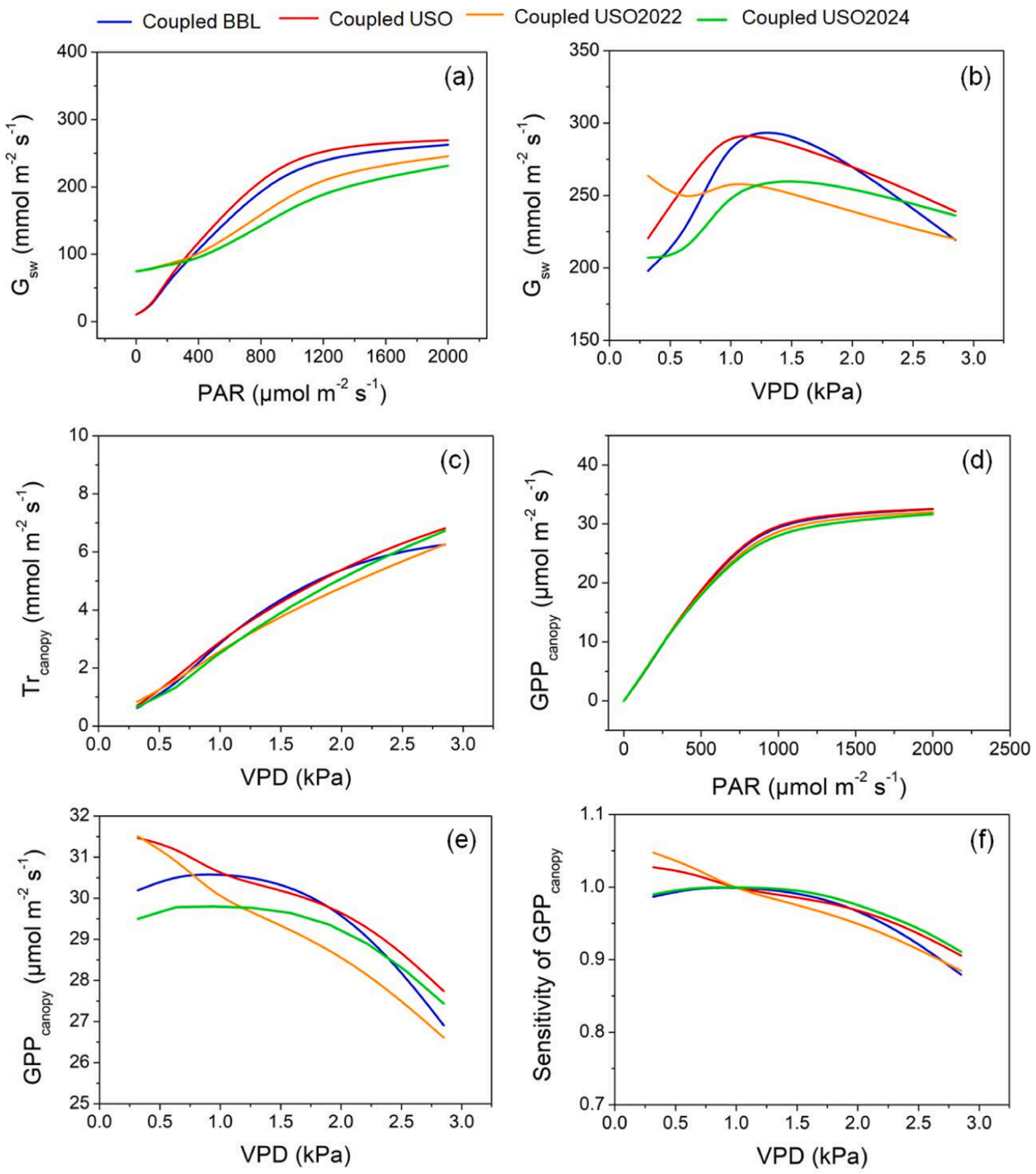

Fig. 8. Response patterns of canopy conductance (G_{sw}, a and b), transpiration rate (Tr_{canopy}, c), and gross primary productivity (GPP_{canopy}, d and e) to PAR and VPD. Subplot (f) exhibits sensitivity of GPP_{canopy} to increasing VPD wherein the GPP_{canopy} value at each VPD was standardized using GPP_{canopy} of VPD = 1.0 kPa (i.e., $GPP_{canopy,VPD}/GPP_{canopy,1.0}$). Response patterns of G_{sw}, Tr_{canopy}, and GPP_{canopy} were generated by using a two-leaf one-layer canopy model with the target predictor variable being changed and other predictor variables held constant. Key parameters employed to drive the canopy model included VPD = 1.0 kPa, T_{air} = 25 °C, CO_2 = 400 ppm, PAR = 1500 μmol m^{-2} s^{-1}, V_{cmax} = 72.0 μmol m^{-2} s^{-1}, J_{max} = 92.0 μmol m^{-2} s^{-1}, g_m = 0.08 mol m^{-2} s^{-1}, LAI = 6.2 m^2 m^{-2}, leaf inclination angle = 10°, and leaf width = 5.0 cm. Temperature response parameters (ΔH_a and ΔS) for V_{cmax}, J_{max}, g_m please refer to Table S2. The slope parameter a_1 and g_0 values refer to Table S3. V_{cmax}: the maximum carboxylation rate; J_{max}: the maximum electron transport rate; g_m: mesophyll conductance; ΔH_a: activation energy; ΔS: entropy of inactivation; LAI: leaf area index.

between the field observations and predictions of the RF, USO2022, and USO2024 models (Fig. 6b). Large differences in absolute values of C_i/C_a were observed at given PAR. Ball and Berry (1982) reported a negative correlation between g_{sw}/A_n and VPD. According to Eq. (10) and the study of Dewar et al. (2018), a decline of g_{sw}/A_n with VPD implies a lower C_i/C_a at high VPD. The lower C_i/C_a values observed in field measurements compared to the predictions of stomatal conductance models could be explained by the higher VPD in the field measurements compared to the parameter settings of the stomatal conductance models.

According to Slot et al. (2016), g_{sw} in sunlit leaves of three tropical tree species from Panama exhibited steep increases at VPD levels below 0.6 kPa, followed by a rapid decline. The g_{sw}-VPD relationship observed in this study using the coupled RF model showed a similar pattern to the findings of Slot et al. These findings suggest that leaf g_{sw} in tropical trees is not infinite at low VPD levels. Initially, when considering transpiration (E) ≈ g_{sw} * VPD, if VPD approaches zero, E also approaches zero. Therefore, the unbounded g_{sw} at low VPD levels was not recognized as a concern (Medlyn et al., 2011; Lamour et al., 2022). They did not realize

the significant overestimation of diurnal g_{sw} at relatively low VPD levels in tropical rainforest trees, which occurs throughout the morning. The quotient values of the $\frac{a_1}{\sqrt{VPD}}$ term in the USO series models exponentially increase at a higher rate as VPD decreases from 1.0 to 0.4 kPa, leading to the issue of unbounded g_{sw}. Modifying the $\frac{a_1}{\sqrt{VPD}}$ term to eliminate the occurrence of low VPD values in the denominator proved effective in limiting the unbounded quotient values at low VPD levels. Specifically, the addition of an empirical coefficient (D_0) in the denominator resulted in a new expression: $\frac{a_1}{\sqrt{VPD+D_0}}$. The quotient values and derivatives of the $\frac{a_1}{\sqrt{VPD+D_0}}$ with respect to VPD exhibit gradual changes at low rates along the VPD axis (Fig. 7a). The value of D_0 was determined based on the monthly mean of the daytime minimum VPD, which adequately accounted for variations in environmental VPD perceived by plants. Moreover, the USO2024 model showed no decrease in prediction accuracy when estimating g_{sw} in high VPD conditions (> 1.0 kPa). The USO2024 model demonstrated comparable accuracy to the USO2022 model when estimating diurnal g_{sw} at high VPD levels (> 2.0 kPa) in Elaeha species in 2021 (Fig. 7b).

The improved USO2024 model demonstrated superior performance exclusively under conditions characterized by low irradiance and low VPD. The USO2024 model is mathematically equivalent to the USO2022 model when D_0 in Eq. (9) is zero. This implies that the USO2022 model is robust for modeling applications in most habitats where the daytime minimum VPD is greater than or equal to 1.0 kPa (Lamour et al., 2022). At the ecosystem level, the Tr_{canopy}-VPD response curve simulated by the USO2024 model was positioned between the simulation results of the USO and USO2022 models (Fig. 8c). It appears that improving the stomatal conductance model at the leaf level could enhance the performance of ecosystem transpiration. However, it should be noted that factors such as canopy structure (e.g., LAI) and climate changes, rather than leaf stomatal physiology, are the most influential determinants of ecosystem functions (Wang et al., 2003; Xue et al., 2017). The main findings from our improved stomatal conductance model could be crucial, depending on the research scales and questions being addressed.

Note that the photosynthesis-RF inference tool had limited capability in providing specific biological parameters, such as the slope parameter of the USO series models. The inability to provide concrete biological parameters may not be a sufficient reason to abandon it. In our research, the photosynthesis-RF inference tool is proved to be useful for investigating and replicating the intricate responses of g_{sw} to environmental factors, including PAR, VPD, T_{leaf}, and CO_2 elevation concentration (*see* note S5).

5. Conclusions

Collectively, the results indicate that the USO model significantly overestimated diurnal g_{sw} at low VPD and irradiance conditions in all sampled tree species partially due to the assumption of a linear correlation between g_{sw} and A_n. Although the performance of the USO2022 model was superior to the USO model, it still overestimated g_{sw} at low VPD levels, mainly because g_{sw} was not bounded. To improve the predictive accuracy of diurnal g_{sw}, a constraint coefficient based on the monthly mean of daytime minimum VPD was added to the USO2022 model, which contributes to substantial improvements in predictive accuracy while retaining g_{sw} response patterns at high VPD.

CRediT authorship contribution statement

Wei Xue: Writing – review & editing, Writing – original draft, Visualization, Conceptualization. **Xue-min He:** Writing – review & editing. **Quan Wang:** Writing – review & editing. **Pei-jun Shi:** Writing – review & editing. **Guang-hui Lv:** Writing – review & editing. **Jian-feng Huang:** Writing – review & editing. **Da Yang:** Writing – review & editing. **Jiao-lin Zhang:** Writing – review & editing, Writing – original draft, Methodology, Funding acquisition, Data curation, Conceptualization.

Declaration of competing interest

The authors declare that they have no known competing financial interests or personal relationships that could have appeared to influence the work reported in this paper.

Data availability

Data are available in the figshare (doi:10.6084/m9.figshare.25442251)

Acknowledgments

The project was supported by the Open Funding from CAS Key Laboratory of Tropical Forest Ecology (22-CAS-TFE-03), Guangzhou collaborative innovation center on science-tech of ecology and landscape (202206010058), and The Leading Talent Program of Xinjiang Uygur Autonomous Region Tianchi Plan (51052401407).

Supplementary materials

Supplementary material associated with this article can be found, in the online version, at doi:10.1016/j.agrformet.2024.110098.

References

Ball, J.T., Berry, J.A., 1982. The C_i/C_s ratio: a basis for predicting stomatal control of photosynthesis. Carnegie Instit. Washington Yearb. 81, 88–92.
Ball, J.T., Woodrow, I.E., Berry, J.A., 1987. A model predicting stomatal conductance and its contribution to the control of photosynthesis under different environmental conditions. In: Biggins, J. (Ed.), Progress in Photosynthesis Research. Springer, Dordrecht, pp. 221–224.
Ball, J.T., 1988. An analysis of stomatal conductance.
Bonan, G.B., Williams, M., Fisher, R.A., Oleson, K.W., 2014. Modeling stomatal conductance in the earth system: linking leaf water-use efficiency and water transport along the soil–plant–atmosphere continuum. Geosci. Model Develop. 7, 2193–2222.
Barnard, D.M., Bauerle, W.L., 2013. The implications of minimum stomatal conductance on modeling water flux in forest canopies. J. Geophys. Res.: Biogeosci. 118, 1322–1333.
Breiman, L., 1996. Bagging predictors. Mach. Learn. 24, 123–140.
Breiman, L., 2001. Random forests. Mach. Learn. 45, 5–32.
Buckley, T.N., 2017. Modeling stomatal conductance. Plant Physiol. 174, 572–582.
Cao, M., Zou, X., Warren, M., Zhu, H., 2006. Tropical forests of Xishuangbanna, China. Biotropica 38, 306–309.
Cao, J., Zhang, Z., Tao, F., Zhang, L., Luo, Y., Han, J., Li, Z., 2020. Identifying the contributions of multi-source data for winter wheat yield prediction in China. Remote Sens. 12, 750.
Cowan, I.R., Farquhar, G.D., 1977. Stomatal function in relation to leaf metabolism and environment. In: Jennings, DH (Ed.), Integration of Activity in the Higher Plant. Cambridge University Press, Cambridge, pp. 471–505.
Cunningham, S.C., 2004. Stomatal sensitivity to vapour pressure deficit of temperate and tropical evergreen rainforest trees of Australia. Trees 18, 399–407.
Damour, G., Simonneau, T., Cochard, H., Urban, L., 2010. An overview of models of stomatal conductance at the leaf level. Plant Cell Environ. 33, 1419–1438.
Davidson, K.J., Julien, D., Rogers, A., Ely, K.S., Li, Q., McDowell, N.G., Pivovaroff, A.L., Wolfe, B.T., Wright, S.J., Zambrano, A., Serbin, S.P., 2023. Short-term variation in leaf-level water use efficiency in a tropical forest. New Phytolog. 237, 2069–2087.
De Kauwe, M.G., Kala, J., Lin, Y.S., Pitman, A.J., Medlyn, B.E., Duursma, R.A., Abramowitz, G., Wang, Y.P., Miralles, D.G., 2015. A test of an optimal stomatal conductance scheme within the CABLE land surface model. Geoscientif. Model Develop. 8, 431–452.
Dewar, R., Mauranen, A., Makela, A., Holtta, T., Medlyn, B., Vesala, T., 2018. New insights into the covariation of stomatal, mesophyll and hydraulic conductances from optimization models incorporating nonstomatal limitations to photosynthesis. New Phytolog. 217, 571–585.
dos Santos, V.A.H.F., Ferreira, M.J., Rodrigues, J.V.F.C., Garcia, M.N., Ceron, J.V.B., Nelson, B.W., Saleska, S.R., 2018. Causes of reduced leaf-level photosynthesis during strong El Niño drought in a Central Amazon forest. Glob. Change Biol. 24, 4266–4279.
Domingues, T.F., Martinelli, L.A., Ehleringer, J.R., 2014. Seasonal patterns of leaf-level photosynthetic gas exchange in an eastern Amazonian rain forest. Plant Ecol. Divers. 7, 189–203.

Egea, G., Verhoef, A., Vidale, P.L., 2011. Towards an improved and more flexible representation of water stress in coupled photosynthesis–stomatal conductance models. Agricult. Forest Meteorol. 151, 1370–1384.
Ehleringer, J.R., Field, C.B., Lin, Z.F., Kuo, C.Y., 1986. Leaf carbon isotope and mineral composition in subtropical plants along an irradiance cline. Oecologia 70, 520–526.
Farquhar, G.D., von Caemmerer, S., Ball, J.A., 1980. A biochemical model of photosynthetic CO_2 assimilation in leaves of C3 species. Planta 149, 78–90.
Farquhar, G.D., Wong, S.C., 1984. An empirical model of stomatal conductance. Austr. J. Plant Physiol. 11, 191–210.
Franks, P.J., Bonan, G.B., Berry, J.A., Lombardozzi, D.L., Holbrook, M., Herold, N., Oleson, K.W., 2018. Comparing optimal and empirical stomatal conductance models for application in Earth system models. Glob. Change Biol. 24, 5708–5723.
Graham, E.A., Mulkey, S.S., Kitajima, K., Phillips, N.G., Wright, S.J., 2003. Cloud cover limits net CO_2 uptake and growth of a rainforest tree during tropical rainy seasons. Proceed. Natl. Acad. Sci. 100, 572–576.
Grossiord, C., Buckley, T.N., Cernusak, L.A., Novick, K.A., Poulter, B., Siegwolf, R.T.W., Sperry, J.S., McDowell, N.G., 2020. Plant responses to rising vapor pressure deficit. New Phytolog. 226, 1550–1566.
Harley, P.C., Tenhunen, J.D., 1991. Modeling the photosynthetic response of C_3 leaves to environmental factors. In: Boote, K.J., Loomis, R.S. (Eds.), Modeling crop photosynthesis-from biochemistry to canopy. Crop Science Society of America, Inc. and America Society of Agromony, Inc., Madison, pp. 17–39.
Han, T., Feng, Q., Yu, T., Yang, X., Zhang, X., Li, K., 2022. Characteristic of stomatal conductance and optimal stomatal behaviour in an arid oasis of Northwestern China. Sustainability 14, 968.
Hirigoyen, A., Acosta-Munoz, C., Salamanca, A.J.A., Varo-Martinez, M.Á., Rachid-Casnati, C., Franco, J., Navarro-Cerrillo, R., 2022. A machine learning approach to model leaf area index in Eucalyptus plantations using high-resolution satellite imagery and airborne laser scanner data. Ann. For. Res. 64, 165–183.
Houborg, R., McCabe, M.F., 2018. A hybrid training approach for leaf area index estimation via cubist and random forests machine-learning. ISPRS J. Photogramm. Remote Sens. 135, 173–188.
Jeong, J.H., Resop, J.P., Mueller, N.D., Fleisher, D.H., Yun, K., Butler, E.E., Timlin, D.J., Shim, K., Gerber, J., S Reddy, V.R., Kim, S., 2016. Random forests for global and regional crop yield predictions. Plos One 11, e0156571.
Jiang, J., Johansen, K., Stanschewski, C.S., Wellman, G., Mousa, M.A.A., Fiene, G.M., Asiry, K.A., Tester, M., McCabe, M.F., 2022. Phenotyping a diversity panel of quinoa using UAV-retrieved leaf area index, SPAD-based chlorophyll and a random forest approach. Precisi. Agricult. 23, 961–983.
Jin, Y., Liao, Z.G., Zhang, Y., Liu, Y., Liu, J.H., Tan, Z.H., 2022. Studies on the flux distribution and energy closure in Xishuangbanna tropical seasonal rainforest, China. J. Trop. Subtrop. Botan. 30, 471–482. In Chinese with English abstract.
Lamour, J., Davidson, K.J., Ely, K.S., Moguédec, G.L., Leakey, A.D.B., Li, Q., Serbin, S.P., Rogers, A., 2022. An improved representation of the relationship between photosynthesis and stomatal conductance leads to more stable estimation of conductance parameters and improves the goodness-of-fit across diverse data sets. Glob. Change Biol. 28, 3537–3556.
Lamour, J., Davidson, K.J., Ely, K.S., Le Moguedec, G., Anderson, J.A., Li, Q.Y., Calderon, O., Koven, C.D., Wright, S.J., Walker, A.P., Serbin, S.P., Rogers, A, 2023. The effect of the vertical gradients of photosynthetic parameters on the CO_2 assimilation and transpiration of a Panamanian tropical forest. New Phytolog. 238, 2345–2362.
Lary, D.J., Alavi, A.H., Gandomi, A.H., Walker, A.L., 2016. Machine learning in geosciences and remote sensing. Geosci. Front. 7, 3–10.
Leuning, R., 1995. A critical appraisal of a combined stomatal-photosynthesis model for C_3 plants. Plant Cell Environ. 18, 339–355.
Lohammar, T., Larsson, S., Linder, S., Falk, S.O., 1980. FAST-simulation models of gaseous exchange in Scots pine. Ecolog. Bull. 32, 505–523.
Li, Q., Serbin, S.P., Lamour, J., Davidson, K.J., Ely, K.S., Rogers, A., 2022. Implementation and evaluation of the unified stomatal optimization approach in the Functionally Assembled Terrestrial Ecosystem Simulator (FATES). Geoscientif. Model Develop. 15, 4313–4329.
Li, Z., Zhang, Y.P., Wang, A., Yuan, G., Yang, Y., Yu, G.R., Sun, X., 2011. Evaluating the models of stomatal conductance response to humidity in a tropical rain forest of Xishuangbanna, southwest China. Hydrol. Res. 42, 307–317.
Lin, Y.S., Medlyn, B.E., Duursma, R.A., Prentice, I.C., Atkin, O.K., Barton, C.V.M., Bennie, J., Bosc, A., Broadmeadow, M.S.J., Cernusak, L.A., Angelis, P.De, Drake, J.E., Eamus, D., Ellsworth, D.S., Freeman, M., Ghannoum, O., Gimeno, T.E.., Han, Q., Hikosaka, K., Hutley, L.B., Kelly, J.W., Kikuzawa, K., Kolari, P., Koyama, K., Limousin, J.M., Linderson, M.L., Löw, M., Macinins-Ng, C., Martin-StPaul, N.K., Meir, P., Mikkelsen, T.N., Mitchell, P., Nippert, J.B., Onoda, Y., de Beeck, M.O., de Dios, V.R, Rey, A., Rogers, A., Rowland, L., Setterfield, S.A., Sun, W., Tarvainen, L., Tausz-Posch, S., Tissue, D.T., Uddling, J., Wallin, G., Warren, J.M., Wingate, L., Zaragoza-Castells, J., 2015. Optimal stomatal behaviour around the world. Nat. Clim. Change 5, 459–464.
Liu, S., Jin, X., Nie, C., Wang, S., Yu, X., Cheng, M., Shao, M., Wang, Z., Tuohuti, N., Bai, Y., Liu, Y., 2021. Estimating leaf area index using unmanned aerial vehicle data: shallow vs. deep machine learning algorithms. Plant Physiol. 187, 1551–1576.
Liu, W., Meng, F.R., Zhang, Y., Liu, Y., Li, H., 2004. Water input from fog drip in the tropical seasonal rain forest of Xishuangbanna, South-West China. J. Trop. Ecol. 20, 517–524.
McCabe, M.F., Rodell, M., Alsdorf, D.E., Miralles, D.G., Uijlenhoet, R., Wagner, W., Lucieer, A., Houborg, R., Verhoest, N.E.C., Franz, T.E., Shi, J., Gao, H., Wood, E.F., 2017. The future of Earth observation in hydrology. Hydrol. Earth Syst. Sci. 21, 3879–3914.
Medlyn, B.E., Berbigier, P., Clement, R., Grelle, A., Loustau, D., Linder, S., Wingate, L., Jarvis, P.G., Sigurdsson, B.D., McMurtrie, R.E., 2005. Carbon balance of coniferous forests growing in contrasting climates: model-based analysis. Agricult. For. Meteorol. 131, 97–124.
Medlyn, B.E., Duursma, R.A., Eamus, Derek., Ellsworth, D.S., Prentice, I.C., Barton, C.V. M., Crous, K.Y., Angelis, P., Freeman, M., Wingate, L., 2011. Reconciling the optimal and empirical approaches to modelling stomatal conductance. Glob. Change Biol. 17, 2134–2144.
Miner, G.L., Bauerle, W.L., Baldocchi, D.D., 2016. Estimating the sensitivity of stomatal conductance to photosynthesis: a review. Plant Cell Environ. 40, 1214–1238.
Ogle, K., Reynolds, J.F., 2002. Desert dogma revisited: coupling of stomatal conductance and photosynthesis in the desert shrub, *Larrea tridentata*. Plant Cell Environ. 25, 909–921.
Oren, R., Sperry, I.S., Katul, G.G., Pataki, D.E., Ewers, B.E., Phillips, N., Schäfer, K.V.R., 1999. Survey and synthesis of intra- and interspecific variation in stomatal sensitivity to vapour pressure deficit. Plant Cell Environ. 22, 1515–1526.
Owen, K.E., Tenhunen, J., Reichstein, M., Wang, Q., Falge, E., Geyer, R., Xiao, X., Stoy, P., Ammann, C., Arain, A., 2007. Linking flux network measurements to continental scale simulations: Ecosystem carbon dioxide exchange capacity under non-water-stressed conditions. Glob. Change Biol. 13, 734–760.
Powell, T.L., Galbraith, D.R., Christoffersen, B.O., Harper, A., Imbuzeiro, H.M.A., Rowland, L., Almeida, S., Brando, P.M., Costa, A.C.L., Costa, M.H., Levine, N.M., Malhi, Y., Saleska, S.R., Sotta, E., Williams, M., Meir, P., Moorcroft, P.R., 2013. Confronting model predictions of carbon fluxes with measurements of Amazon forests subjected to experimental drought. New Phytolog. 200, 350–365.
Reichstein, M., Camps-Valls, G., Stevens, B., Jung, M., Denzler, J., Carvalhais, N., 2019. Deep learning and process understanding for data-driven Earth system science. Nature 566, 195–204.
Rogers, A., Medlyn, B.E., Dukes, J.S., Bonan, G., von Caemmerer, S., Dietze, M.C., Kattge, J., Leakey, A.D.B., Mercado, L.M., Niinemets, Ü., Prentice, I.C., Serbin, S.P., Sitch, S., Way, D.A., Zaehle, S., 2017. A roadmap for improving the representation of photosynthesis in Earth system models. New Phytolog. 213, 22–42.
Rogers, A., Kumarathunge, D.P., Lombardozzi, D.L., Medlyn, B.E., Serbin, S.P., Walker, A.P., 2021. Triose phosphate utilization limitation: an unnecessary complexity in terrestrial biosphere model representation of photosynthesis. New Phytolog. 230, 17–22.
Saunders, A., Drew, D.M., Brink, W., 2021. Machine learning models perform better than traditional empirical models for stomatal conductance when applied to multiple tree species across different forest biomes. Tree. For. People 6, 100139.
Slot, M., Garcia, M.N., Winter, K., 2016. Temperature response of CO_2 exchange in three tropical tree species. Funct. Plant Biol. 43, 468–478.
Tuzet, A., Perrier, A., Leuning, R., 2003. A coupled model of stomatal conductance, photosynthesis and transpiration. Plant Cell Environ. 26, 1097–1116.
Vidale, P.L., Egea, G., McGuire, P.C., Todt, M., Peters, W., Müller, O., Balan-Sarojini, B., Verhoef, A., 2021. On the treatment of soil water stress in GCM simulations of vegetation physiology. Front. Environ. Sci. 9.
Wang, Y.P., Leuning, R., 1998. A two-leaf model for canopy conductance, photosynthesis and partitioning of available energy I. Model description and comparison with a multi-layered model. Agricult. For. Meteorol. 91, 89–111.
Wang, Q., Tenhunen, J., Falge, E., Bernhofer, C., Granier, A., Vesala, T., 2003. Simulation and scaling of temporal variation in gross primary production for coniferous and deciduous temperate forests. Glob. Change Biol. 10, 37–51.
Wong, S.C., Cowan, I.R., Farquhar, G.D., 1978. Leaf conductance in relation to assimilation in *Eucalyptus pauciflora* Sieb. ex Spreng. Plant Physiol. 62, 670–674.
Wu, J., Serbin, S.P., Ely, K.S., Wolfe, B.T., Dickman, L.T., Grossiord, C., Michaletz, S.T., Collins, A.D., Detto, M., McDowell, N.G., Wright, S.J., Rogers, A., 2020. The response of stomatal conductance to seasonal drought in tropical forests. Glob. Change Biol. 26, 823–839.
Xue, W, Jeong, S., Ko, J.H., Tenhunen, J., 2017. Linking canopy reflectance to crop structure and photosynthesis to capture and interpret spatiotemporal dimensions of per-field photosynthetic productivity. Biogeosciences 14, 1315–1332.
Xue, W., Lindner, S., Nay-Htoon, B., Dubbert, M., Otieno, D., Ko, J., Muraoka, H., Werner, C., Tenhunen, J., Harley, P., 2016. Nutritional and developmental influences on components of rice crop light use efficiency. Agricult. For. Meteorol. 223, 1–16.
Xue, W, Luo, H., Carriquí, M., Nadal, M., Huang, J., Zhang, J., 2022. Quantitative expression of mesophyll conductance temperature response in the FvCB model and impacts on plant gas exchange estimations. Agricult. For. Meteorol. 325, 109153.
Zhang, L.G., Yu, S., An, D., Sun, Q., Luo, W., Yin, X., 2017. Can the responses of photosynthesis and stomatal conductance to water and nitrogen stress combinations be modeled using a single set of parameters? Front. Plant Sci. 8, 328.
Zhi, J.J., Cao, X.Y., Zhang, Z.H., Qin, T.T., Qu, L., Qi, L.Y., Ge, L.W., Guo, A.X., Wang, X. T., Da, C., Sun, Y., Liu, W.B., Zhang, H.M., Fu, X.W., 2022. Identifying the determinants of crop yields in China since 1952 and its policy implications. Agricult. For. Meteorol. 327, 109216.